September 19-22, 2018, Svetlogorsk, Russia

AEROACOUSTIC CHARACTERIZATION OF TURBO-MACHINERY

Mats Åbom

KTH-The Royal Inst of Technology
The **M**arcus **W**allenberg **L**aboratory
for Sound and Vibration Research (MWL)
SE-100 44 Stockholm, Sweden

matsabom@kth.se
orcid.org/0000-0001-7898-8643

ROYAL INSTITUTE OF TECHNOLOGY

MWL group at KTH Campus 2016

Content

- Background
- Acoustic installation effects
- Aeroacoustic Multi-ports
- Experimental/Numerical characterization
- Examples of Numerical Multi-port work at KTH
- Summary

Reference List

BACKGROUND

Aeroacoustics - Started around 1950´s related to noise issues with the then new jet powered civil aircrafts…

$$\frac{1}{c_0^2}\frac{\partial^2 p'}{\partial t^2} - \nabla^2 p' = s$$

Lighthills acoustic analogy

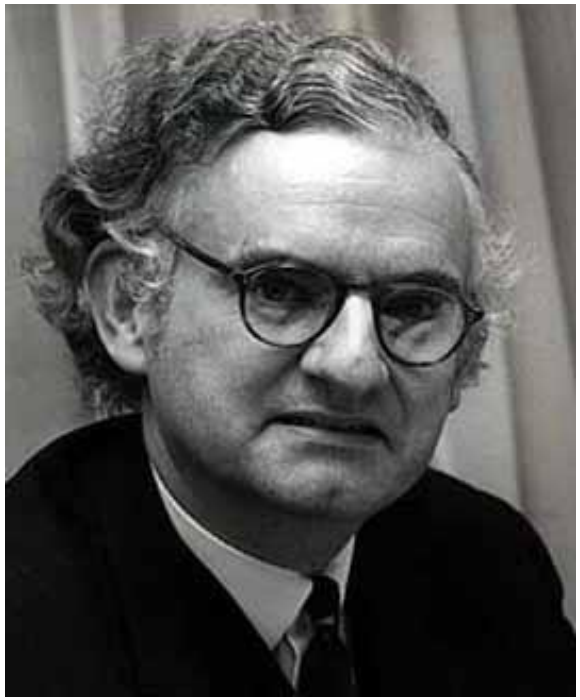

Sir Michael JAMES Lighthill FRS

(1924-1998)

Limitations in Lighthill´s theory

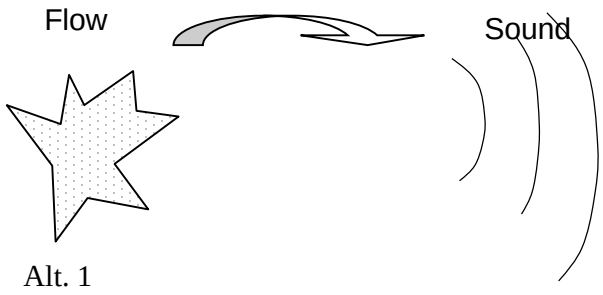

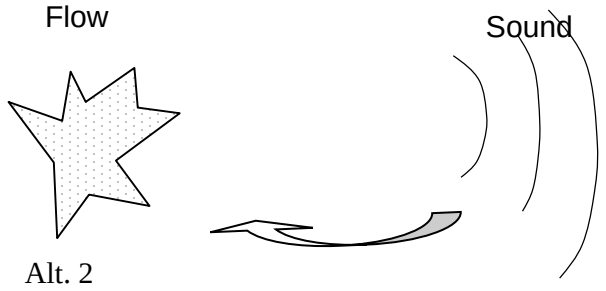

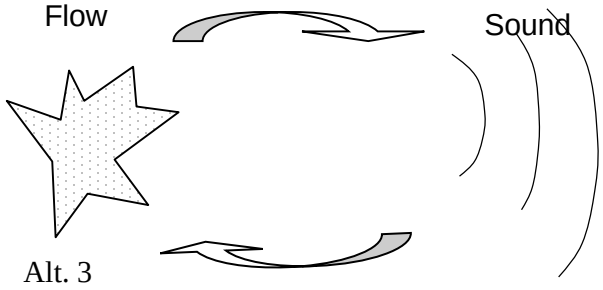

Alt. 1: Sound production by a flow.

Alt. 2: Sound-vortex interaction (dissipation/ amplification).

Alt. 3: Whistling (Non-linear Aero-Acoustics)

Limitations in Lighthill´s theory

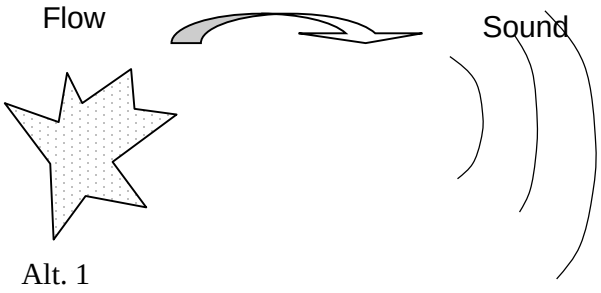

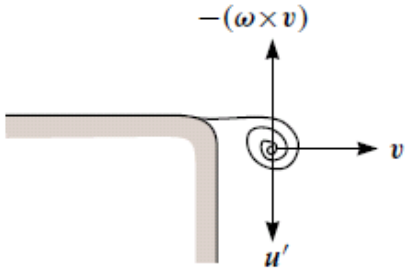

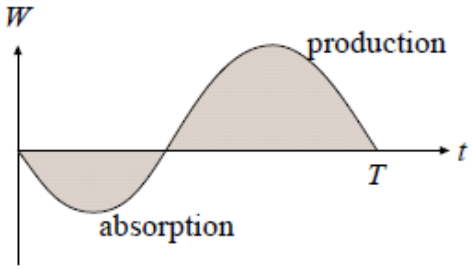

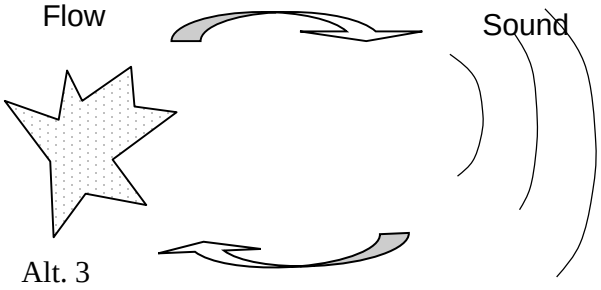

Alt. 1: Sound production by a flow.

Alt. 2: Sound-vortex interaction (dissipation/ amplification).

Alt. 3: Whistling (Non-linear Aero-Acoustics)

Limitations in Lighthill´s theory

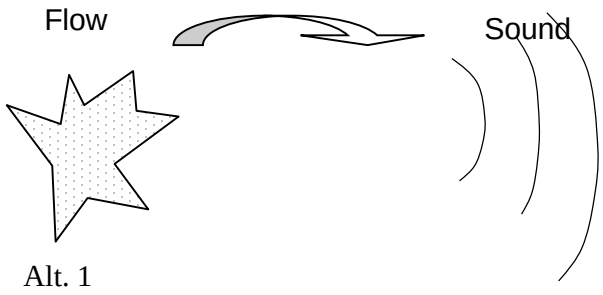

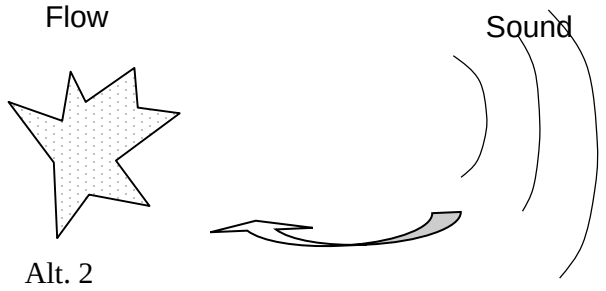

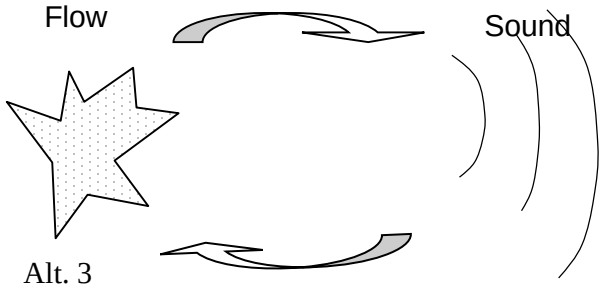

Lighthill or linear Aero-Acoustics is OK

Alt. 1: Sound production by a flow.

Alt. 2: Sound-vortex interaction (dissipation/ amplification).

Alt. 3: Whistling (Non-linear Aero-Acoustics)

ACOUSTIC INSTALLATION EFFECTS ("No free-field")

- In the low frequency (plane wave) range ($f < f_{cut\text{-}on}$) a source is strongly coupled to a system and the acoustic output (power) can vary strongly.

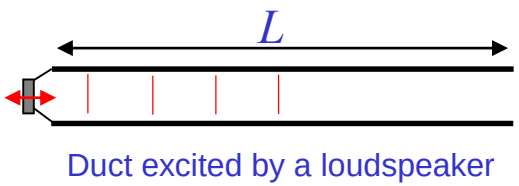

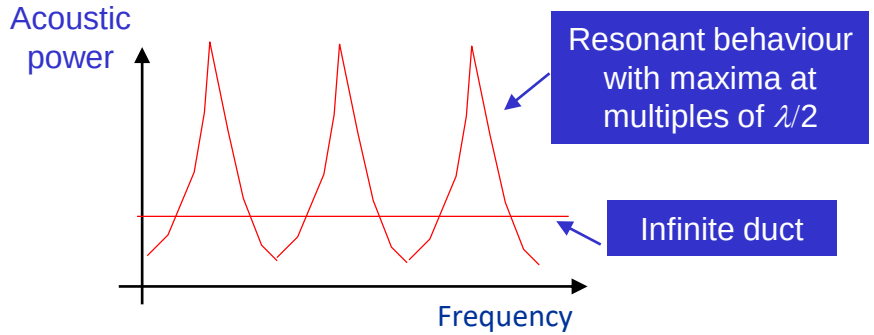

- In the mid frequency range up to (2-3)x $f_{cut\text{-}on}$, *plane + non-plane waves* exist. Also in this range strong coupling between source and system is possible.

- In the high frequency range $f > 3xf_{cut\text{-}on}$, sound propagates as rays, there is no coupling between a source and a system and the acoustic power equals the free field value.

ACOUSTIC INSTALLATION EFFECTS ("No free-field")

- In the low frequency (plane wave) range ($f < f_{cut\text{-}on}$) a source is strongly coupled to a system and the acoustic output (power) can vary strongly.

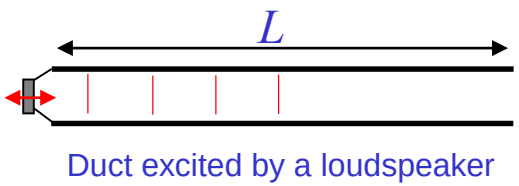

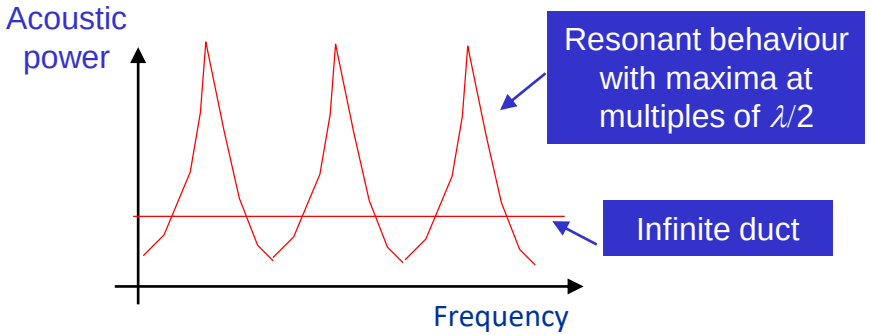

- In the mid frequency range up to (2-3)x $f_{cut\text{-}on}$, *plane + non-plane waves* exist. Also in this range strong coupling between source and system is possible.

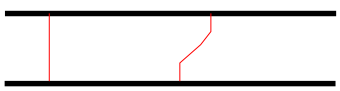

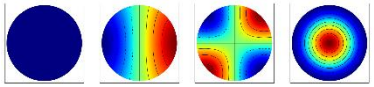

- In the high frequency range $f > 3xf_{cut\text{-}on}$, sound propagates as rays, there is no coupling between a source and a system and the acoustic power equals the free field value.

ACOUSTIC INSTALLATION EFFECTS ("No free-field")

Coupled models required

- In the low frequency (plane wave) range ($f < f_{cut\text{-}on}$) a source is strongly coupled to a system and the acoustic output (power) can vary strongly.

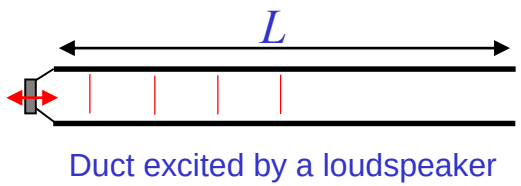

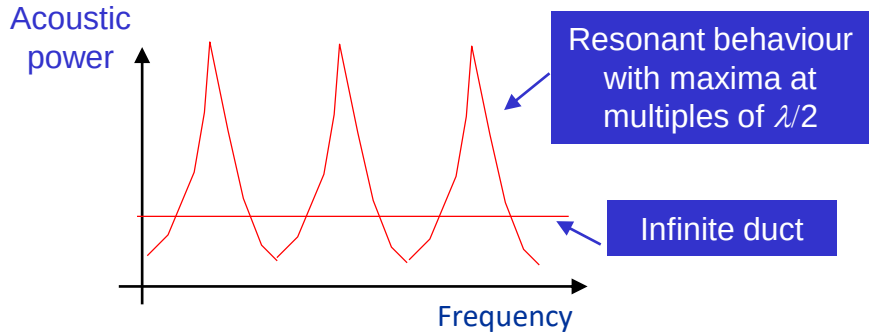

- In the mid frequency range up to (2-3)x $f_{cut\text{-}on}$, *plane + non-plane waves* exist. Also in this range strong coupling between source and system is possible.

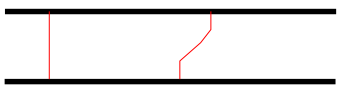

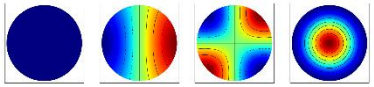

- In the high frequency range $f > 3xf_{cut\text{-}on}$, sound propagates as rays, there is no coupling between a source and a system and the acoustic power equals the free field value.

ACOUSTIC INSTALLATION EFFECTS ("No free-field")

Coupled models required

- In the low frequency (plane wave) range ($f < f_{cut\text{-}on}$) a source is strongly coupled to a system and the acoustic output (power) can vary strongly.

In practice the limit is around ~ 10 propagating modes or:

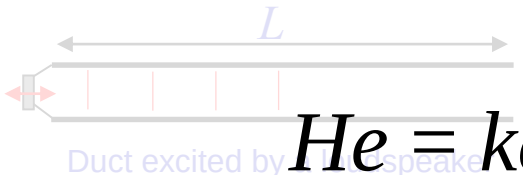

$$He = kd < 3\pi,$$

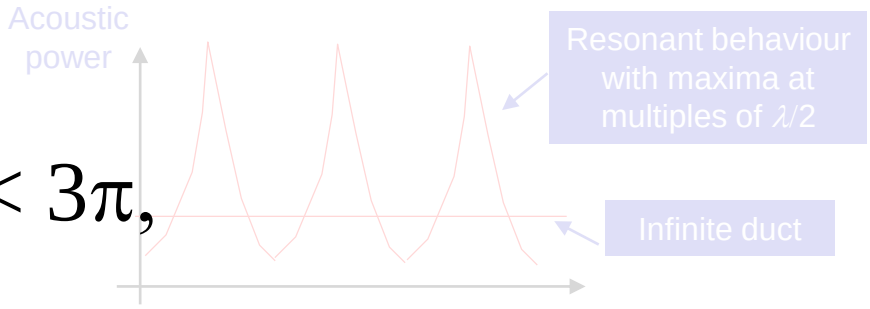

where k is the wave-number and d the duct diameter.

- In the mid frequency range up to (2-3)x $f_{cut\text{-}on}$, *plane + non-plane waves* exist. Also in this range strong coupling between source and system is possible.

- In the high frequency range $f > 3xf_{cut\text{-}on}$, sound propagates as rays, there is no coupling between a source and a system and the acoustic power equals the free field value.

AEROACOUSTIC MULTI-PORTS [1-5,11]

The sound field in a duct can be expanded in propagating waves or modes:

Ψ_n:

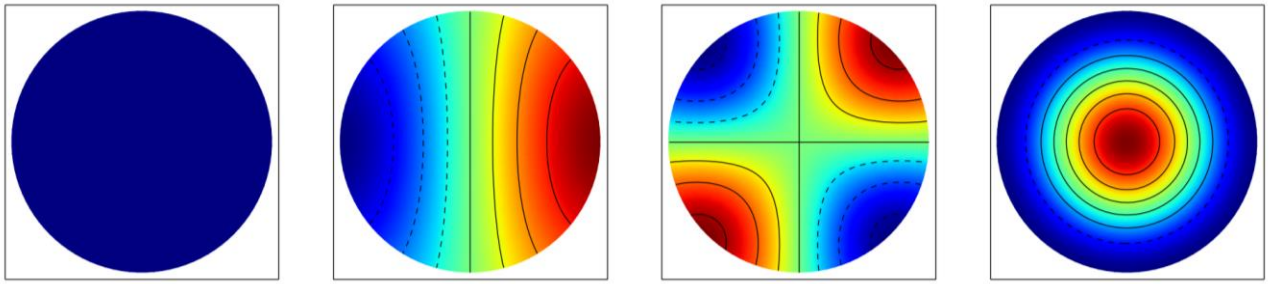

$$\hat{p}(x,y,z) = \sum_{n=0}^{N-1} \left(\hat{p}_{+n} \Psi_n(x,y) \exp(-ik_{+z,n} z) + \hat{p}_{-n} \Psi_n(x,y) \exp(ik_{-z,n} z) \right)$$

where N is at least the number of cut-on modes and z the duct axis.

AEROACOUSTIC MULTI-PORTS [1-5,11]

The sound field in a duct can be expanded in propagating waves or modes:

Ψ_n:

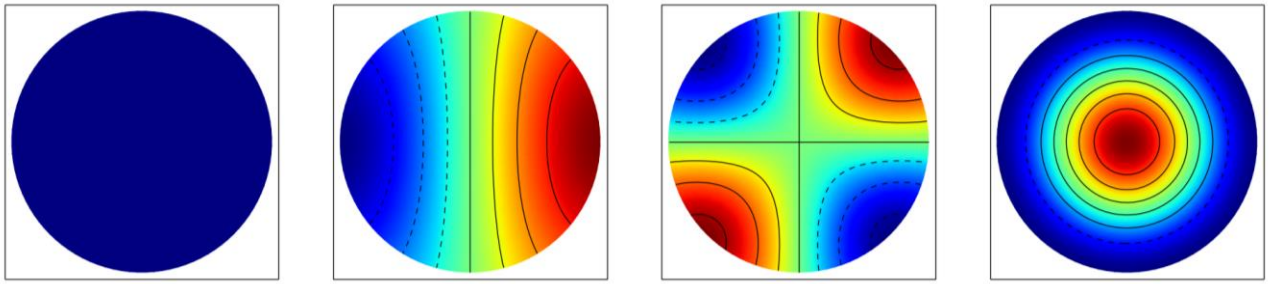

$\hat{p}($ $)$

The eigenmodes can be based on a rigid walled duct and a plug flow forming a complete functional basis. The axial wave-number should include visco-thermal losses as described e.g. by: C Weng, F Bake (2016), Acta Acustica united Acustica 102(6), 1138-1141.

AEROACOUSTIC MULTI-PORTS [1-5,11]

The sound field in a duct can be expanded in propagating waves or modes:

Ψ_n:

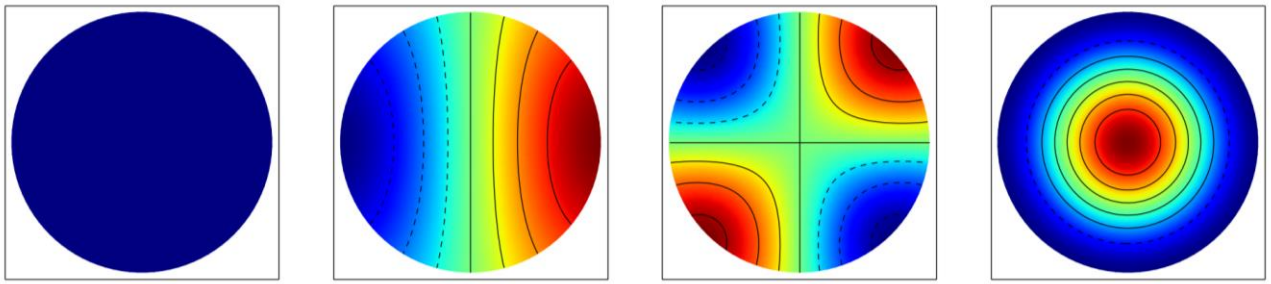

Assuming we sample the field at $M \geq 2N$ points in space we can write:

$$\left(\hat{p}_m\right) = \left[M_{mn}\right] \begin{pmatrix} \left(\hat{p}_{+n}\right) \\ \left(\hat{p}_{-n}\right) \end{pmatrix}, \; M_{mn} = \Psi_n(x_m, y_m) \exp(\mp i k_{\pm z,n} z_m)$$

AEROACOUSTIC MULTI-PORTS [1-5,11]

The sound field in a duct can be expanded in propagating waves or modes:

Ψ_n:

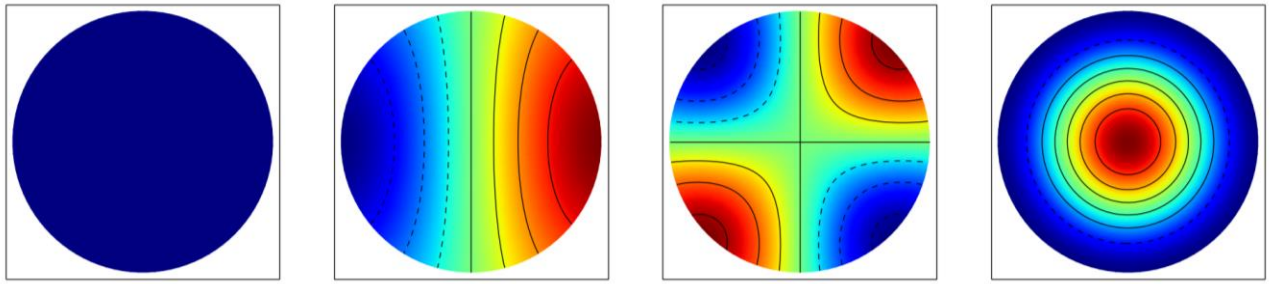

This is the basis for so called **wave decomposition methods**:

$$\mathbf{p} = \mathbf{M}\begin{pmatrix}\mathbf{p}_+\\ \mathbf{p}_-\end{pmatrix} \Rightarrow \begin{pmatrix}\mathbf{p}_+\\ \mathbf{p}_-\end{pmatrix} = \mathbf{M}^{-1}\mathbf{p}$$

The accuracy will depend on the condition number of **M**, i.e., the sampling positions.

Example: Circular duct 6 modes

Condition number: $\mathrm{cond}(\mathbf{M}) = \|\mathbf{M}\| \cdot \|\mathbf{M}^{-1}\|$

Weak singularities: $|z_2 - z_1| = l\frac{\lambda_n}{2}$ $\quad \frac{\theta_2}{\theta_1} = \frac{\pi}{m} l \quad l = 1, 2, 3, \ldots$

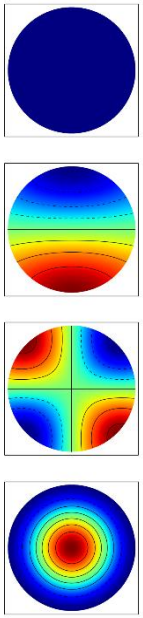

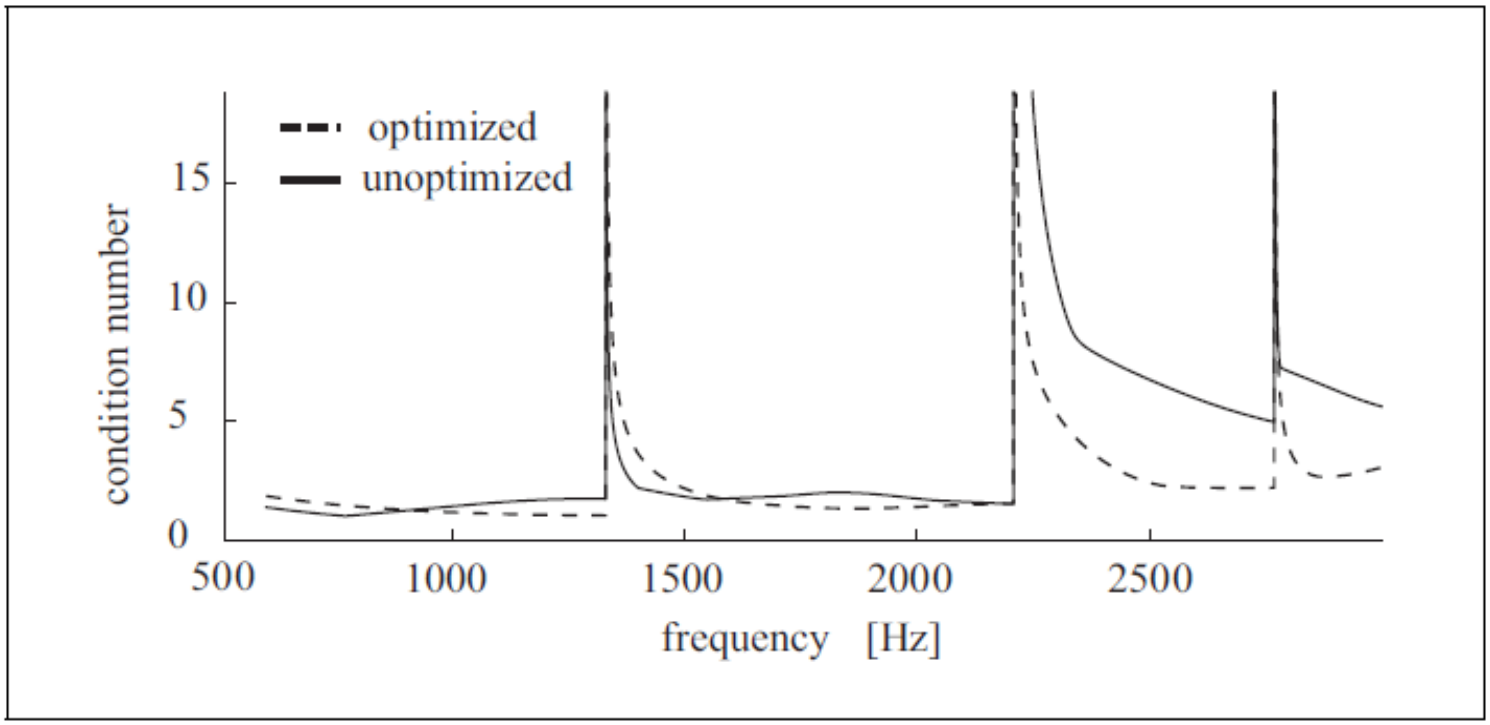

From Ref. [11] showing the effect of optimization on a configuration of 12 flush mounted microphones.

AEROACOUSTIC MULTI-PORTS [1-5,11]

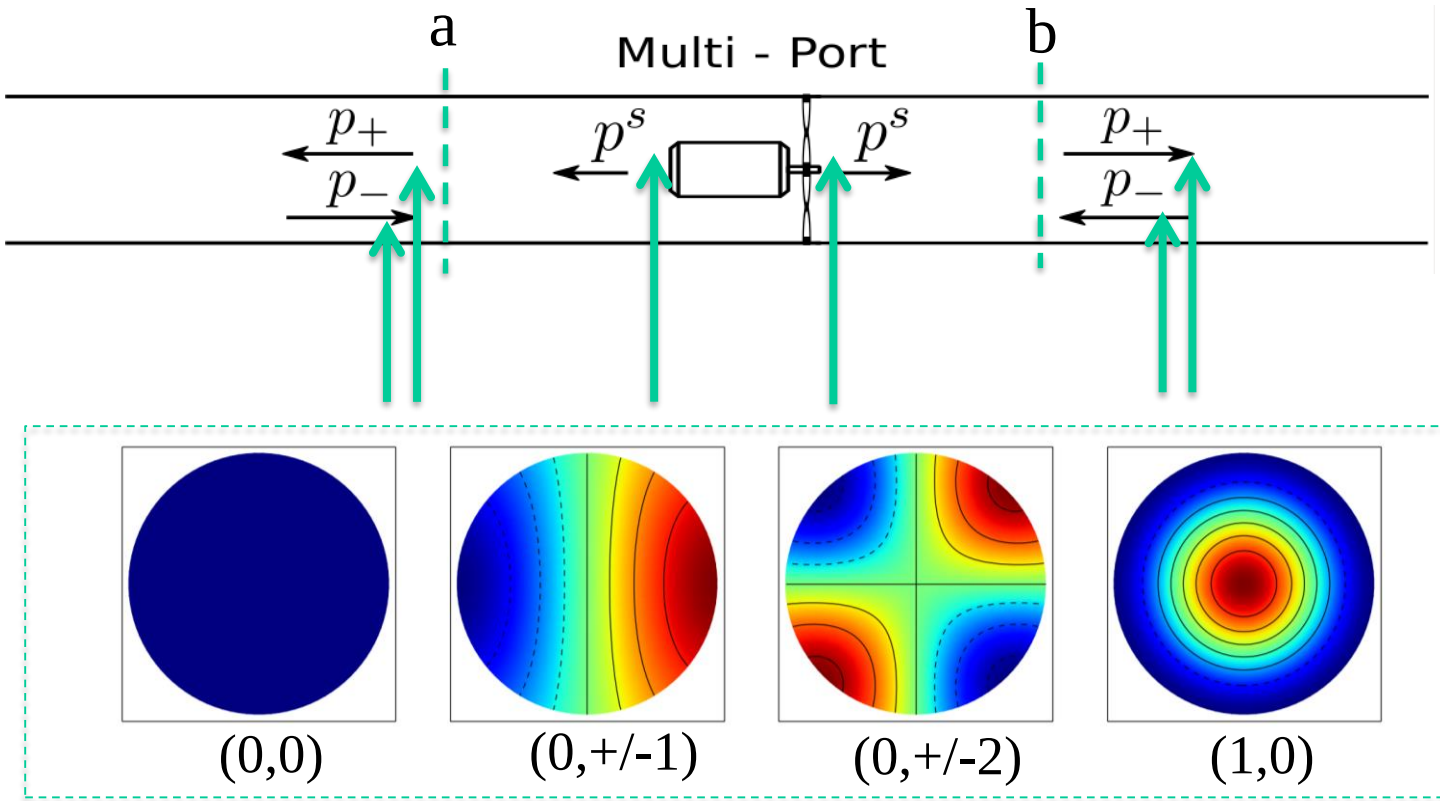

The Multi-port relates the amplitudes for modes at two (or several) **Reference cross-sections** (a&b).

AEROACOUSTIC MULTI-PORTS [1-5,11]

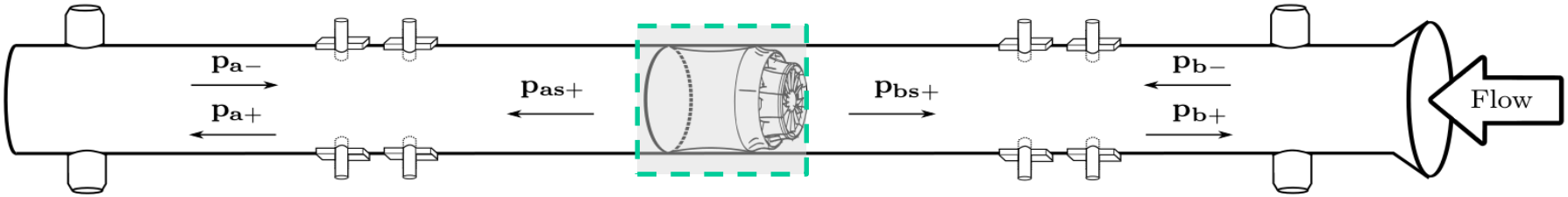

Assume **linear** and **time-invariant** systems then a multi-port in a duct can in (the Fourier domain) be characterized by

$$\underbrace{\begin{bmatrix} \mathbf{p}_{a+} \\ \mathbf{p}_{b+} \end{bmatrix}}_{\mathbf{p}_+} = \underbrace{\begin{bmatrix} \mathbf{R}_{11} & \mathbf{T}_{12} \\ \mathbf{T}_{21} & \mathbf{R}_{22} \end{bmatrix}}_{\mathbf{S}=\text{Passive Part}} \cdot \underbrace{\begin{bmatrix} \mathbf{p}_{a-} \\ \mathbf{p}_{b-} \end{bmatrix}}_{\mathbf{p}_-} + \underbrace{\begin{bmatrix} \mathbf{p}^s_{a+} \\ \mathbf{p}^s_{b+} \end{bmatrix}}_{\mathbf{p}^s_+=\text{Active (Source) Part}}$$

Reflection/transmission of sound

where $\mathbf{p}_{+/-}$ represent travelling modal pressure amplitudes and **S** is the **scattering matrix** and $\mathbf{p}^s$ represents the **source part**.

AEROACOUSTIC MULTI-PORTS [1-5,11]

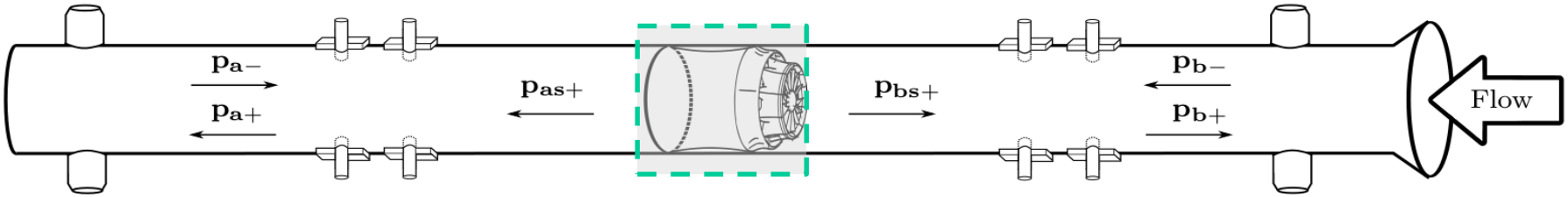

Loudspeakers Mics. **Black-box model** Mics. Loudspeakers

Assume linear and time-invariant systems then a multi-port in a duct can in (the Fourier domain) be characterized by

$$\underbrace{\begin{bmatrix} \mathbf{p}_{a+} \\ \mathbf{p}_{b+} \end{bmatrix}}_{\mathbf{p}_+} = \underbrace{\begin{bmatrix} \mathbf{R}_{11} & \mathbf{T}_{12} \\ \mathbf{T}_{21} & \mathbf{R}_{22} \end{bmatrix}}_{\mathbf{S}=\text{Passive Part}} \cdot \underbrace{\begin{bmatrix} \mathbf{p}_{a-} \\ \mathbf{p}_{b-} \end{bmatrix}}_{\mathbf{p}_-} + \underbrace{\begin{bmatrix} \mathbf{p}^s_{a+} \\ \mathbf{p}^s_{b+} \end{bmatrix}}_{\mathbf{p}^s_+=\text{Active (Source) Part}}$$

Reflection/transmission of sound

CREMER L. (1971) "The second annual Fairey lecture: The treatment of fans as black boxes", J. Sound Vib., 16, 1-15.

AEROACOUSTIC MULTI-PORTS [1-5,11]

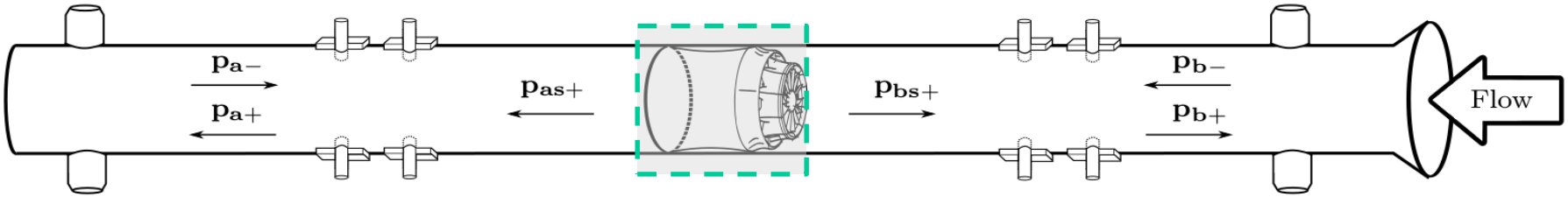

Assume linear and time-invariant systems then a multi-port in a duct can in (the Fourier domain) be characterized by

N.B. The Scattering matrix contains vortex-sound effects

$$\mathbf{p}_+ = \mathbf{S}\,\mathbf{p}_- + \mathbf{p}_+^s$$

Reflection-free source data

where $\mathbf{p}_{+/-}$ represent travelling modal pressure amplitudes and $\mathbf{S}_0$ is the **scattering matrix** and $\mathbf{p}^s$ represents the **source part**.

Advantages (Experimental/Numerical) of the Multi-Port Method

- Projecting the pressure field on the acoustic modes will **suppress Hydrodynamic pressure fluctuations**
- **The effects of boundary conditions are eliminated** i.e. reflection free source data can be determined
- Complex systems can be broken down into sub-elements each described by a multi-port

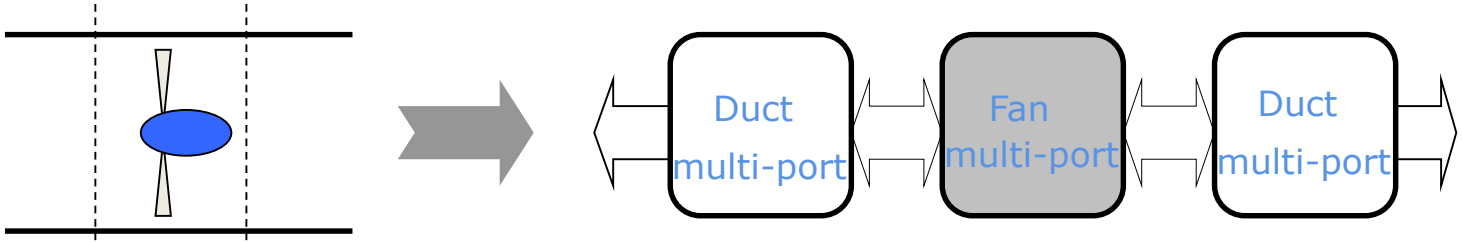

Advantages (Experimental/Numerical) of the Multi-Port Method

- **The effects of boundary conditions are eliminated** i.e. reflecti
- Project nodes will also **su tuations**
- Compl b-elements each described by a multi-port

In practice the full multi-port approach is restricted to the low- and mid-frequency range or (say) 10 modes

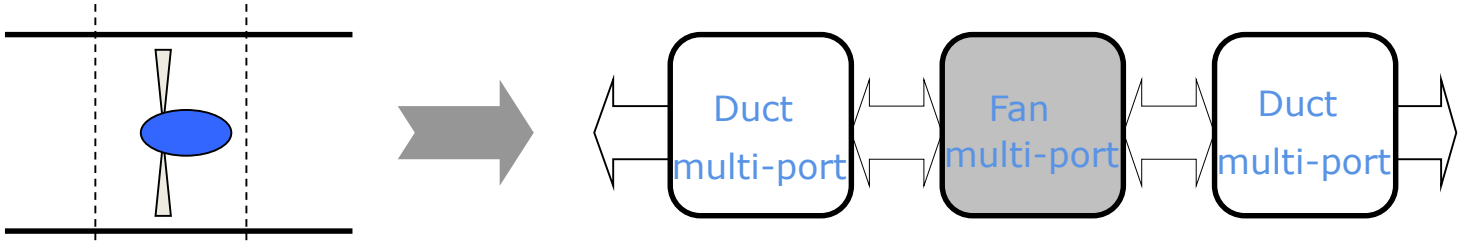

EXPERIMENTAL/NUMERICAL CHARACTERIZATION [1-14]

1) Test the multi-port using N different incident fields and measure **p**+ and **p**- for each case this gives an equation for the scattering-matrix $\mathbf{S}$

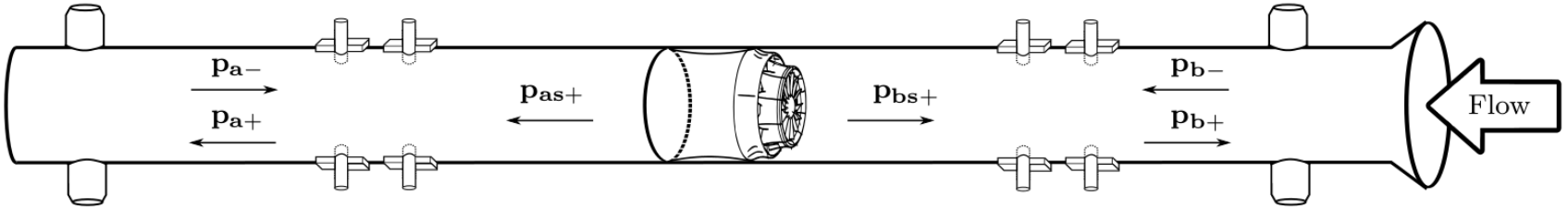

$$\mathbf{p}_+ = \mathbf{S}\,\mathbf{p}_- + \mathbf{p}_+^{s}$$

EXPERIMENTAL/NUMERICAL CHARACTERIZATION [1-14]

1. Test the multi-port using N different incident fields and measure **p**+ and **p**- for each case this gives an equation for the scattering-matrix $\mathbf{S}$

$$\left[\mathbf{p}_{0+}\ \mathbf{p}_{2+}\cdots\mathbf{p}_{(N-1)+}\right]=\mathbf{S}\left[\mathbf{p}_{0-}\ \mathbf{p}_{2-}\cdots\mathbf{p}_{(N-1)-}\right]$$

where the pressure data should be **uncorrelated** with the external source to supress $\mathbf{p}_{+}^{s}$

2. Once S_0 is known the source strength can be directly determined from

$$\mathbf{p}_{s+}=\mathbf{p}_{+}-\mathbf{S}\mathbf{p}_{-}$$

3. This is used to estimate the source cross-spectrum matrix

$$\mathbf{G}_{ss}=E\left[\mathbf{p}_{s+}\mathbf{p}_{s+}^{c}\right]$$

EXPERIMENTAL/NUMERICAL CHARACTERIZATION [1-14]

1. Test the multi-port using N different incident fields and measure **p**+ and **p**- for each case this gives an equation for the scattering-matrix $\mathbf{S}$

$$\left[\mathbf{p}_{0+}\ \mathbf{p}_{2+}\cdots\mathbf{p}_{(N-1)+}\right]=\mathbf{S}\left[\mathbf{p}_{0-}\ \mathbf{p}_{2-}\cdots\mathbf{p}_{(N-1)-}\right]$$

where the pressure data should be correlated with the external source to supress $\mathbf{p}_{+}^{s}$

2. Once $\mathbf{S}$ is known the source strength can be directly determined from

$$\mathbf{p}_{s+}=\mathbf{p}_{+}-\mathbf{S}\mathbf{p}_{-}$$

3. This is used to estimate the source cross-spectrum matrix

$$\mathbf{G}_{ss}=E\left[\mathbf{p}_{s+}\mathbf{p}_{s+}^{c}\right]$$

EXPERIMENTAL/NUMERICAL CHARACTERIZATION [1-14]

1. Test the multi-port using N different incident fields and measure **p**+ and **p**- for each case this gives an equation for the scattering-matrix $\mathbf{S}$

$$\left[\mathbf{p}_{0+}\ \mathbf{p}_{2+}\cdots\mathbf{p}_{(N-1)+}\right]=\mathbf{S}\left[\mathbf{p}_{0-}\ \mathbf{p}_{2-}\cdots\mathbf{p}_{(N-1)-}\right]$$

where the pressure data should be correlated with the external source to supress $\mathbf{p}_{+}^{s}$

2. Once $\mathbf{S}$ is known the source strength can be directly determined from

$$\mathbf{p}_{s+}=\mathbf{p}_{+}-\mathbf{S}\mathbf{p}_{-}$$

3. This is used to estimate the source cross-spectrum matrix

$$\mathbf{G}_{ss}=E\left[\mathbf{p}_{s+}\mathbf{p}_{s+}^{c}\right]$$

EXPERIMENTAL/NUMERICAL CHARACTERIZATION [1-14]

4. For low Mach-cases the determination of the source data will suffer from bad S/N ratios. To improve this correlation with sets >=2N points in each is used

$$\mathbf{p}_{s+} = \mathbf{T}_k \mathbf{p}_{s+,k}$$

where $\mathbf{T}$ is a transfer-matrix moving the data to the reference cross-sections (a & b).

5. For experimental determination one is limited by the number of pressure probes. A solution is then to measure the reflection matrix $\mathbf{R}$ for the test rig which leads to

$$\mathbf{p}_{s+} = (\mathbf{E} - \mathbf{SR})\mathbf{p}_{+} = \underbrace{(\mathbf{E} - \mathbf{SR})(\mathbf{E} + \mathbf{R})^{-1}}_{\mathbf{C}} \mathbf{p}$$

This formulation only requires sets with >= N data points on each side.

EXPERIMENTAL/NUMERICAL CHARACTERIZATION [1-14]

4. For low Mach-cases the determination of the source data will suffer from bad S/N ratios. To improve this correlation with sets >=2N points in each is used

$$\mathbf{p}_{s+} = \mathbf{T}_k \mathbf{p}_{s+,k}$$

where $\mathbf{T}$ is a transfer-matrix moving the data to the reference cross-sections (a & b).

5. For experimental determination one is limited by the number of pressure probes. A solution is then to measure the reflection matrix $\mathbf{R}$ for the test rig which leads to

$$\mathbf{p}_{s+} = (\mathbf{E} - \mathbf{SR})\mathbf{p}_{+} = \underbrace{(\mathbf{E} - \mathbf{SR})(\mathbf{E} + \mathbf{R})^{-1}}_{\mathbf{C}}\mathbf{p}$$

This formulation only requires sets with >= N data points on each side.

COMPARISON EXPERIMENTAL versus NUMERICAL CHARACTERIZATION

1. In **experiments** only **pressure data at the walls** are normally possible to measure.

2. In **simulations all points** can be used AND also **all fields** are known. This means wave decomposition can be based on pressure and e.g. axial velocity.

3. In **experiments** only **wall mounted sources** are normally used to determine the scattering, which makes excitation of single modes difficult. In **simulations** excitation of **single incident modes** is no problem.

4. In experiments a **low S/N** in source strength data can be handled by using a **long measurement time**. For **simulations** normally only a **short time record** is possible (~1 s). **BUT a very large number of sampling points are available**.

EXAMPLES OF NUMERICAL MULTI-PORT WORKS AT KTH

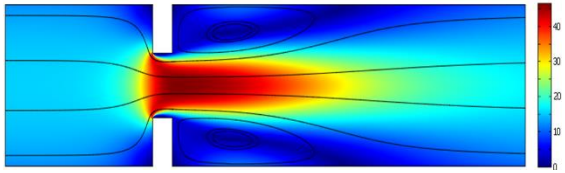

Single Orifice – **i)** Linearized Navier Stokes Equations (LNSE) – 2-port Scattering matrix & Whistling analysis; **ii)** LES – Complete 2-port. [7-9]

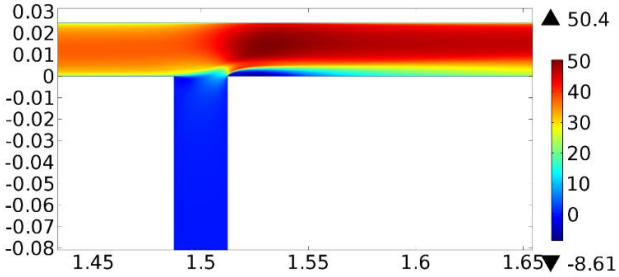

T-junction – LNSE model 3-port Scattering matrix-Sound amplification. [10]

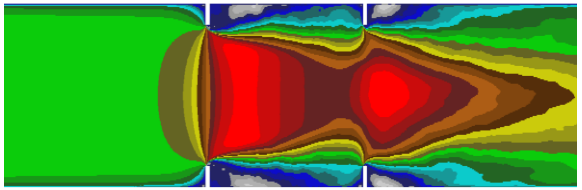

Tandem orifice configuration – Complete multi-port up to the radial mode (=6 modes); *Hybrid model* - Scattering using LNSE, Sound generation using hybrid RANS&LES (IDDES). [13,14]

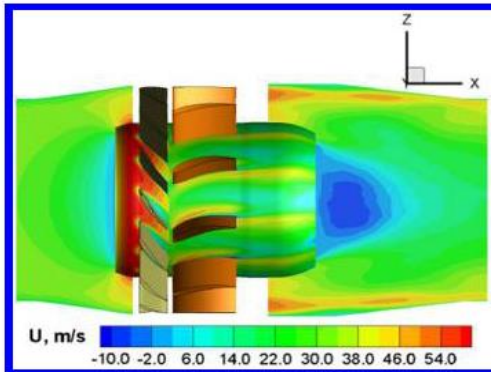

Axial compressor – Modal Source spectra using IDDES. [12]

Single Orifice i) Plane wave scattering and whistling using LNSE [7]

M = 0.044, c=343 m/s

$Re_H = 2.5 \cdot 10^4$

Steady-state Reynolds-Averaged Navier-Stokes (RANS)

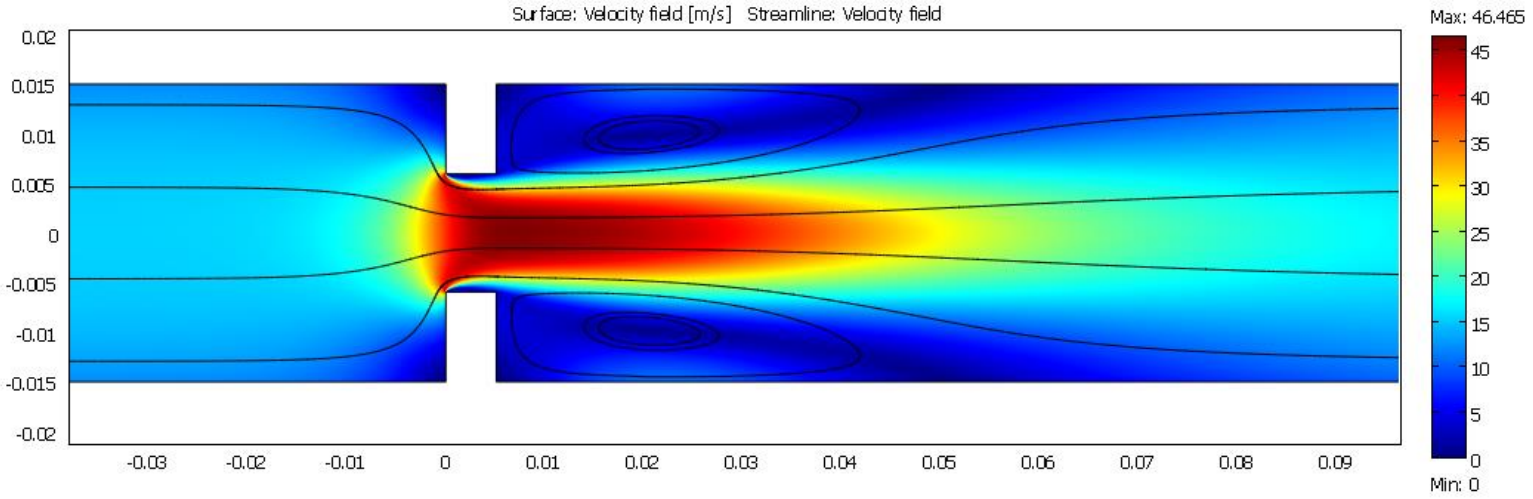

Duct diameter 30 mm; Thick orifice plate, 5 mm; Area contraction ratio = 0.4

Might amplify sound!

Governing equations [6]

Start with non-linear compressible
Navier-Stokes equations.

Assumptions

Linearize.

Assume isentropic process and put $p'=c^2\rho'$.

$\longrightarrow$ Energy eq. is disconnected from N-S eqs.

Frequency domain $e^{-i\omega t}$.

2D geometry.

Linearized Navier-Stokes eqs. [6]

$$\hat{\rho}: \quad \nabla \cdot (-\varepsilon_1 \nabla \hat{\rho}) \; + \; (\hat{u}_0 \; \hat{v}_0) \cdot \nabla \hat{\rho} + \left(\frac{\partial \hat{u}_0}{\partial x} \; + \; \frac{\partial \hat{v}_0}{\partial y} - i\omega \right) \hat{\rho} \; = \; - \left(\frac{\partial \hat{\rho}_0 \hat{u}}{\partial x} + \frac{\partial \hat{\rho}_0 \hat{v}}{\partial y} \right)$$

$$\hat{u}: \quad \nabla \cdot \left(- \begin{pmatrix} \frac{4}{3}\mu + \varepsilon_2 & 0 \\ 0 & \mu + \varepsilon_2 \end{pmatrix} \nabla \hat{u} \right) \; + \; \hat{\rho}_0 (\hat{u}_0 \; \hat{v}_0) \cdot \nabla \hat{u} + \hat{\rho}_0 \left(\frac{\partial \hat{u}_0}{\partial x} - i\omega \right) \hat{u} \; =$$

$$= F - \left(\hat{u}_0 \frac{\partial \hat{u}_0}{\partial x} + \hat{v}_0 \frac{\partial \hat{u}_0}{\partial y} \right) \hat{\rho} - \frac{\partial c^2 \hat{\rho}}{\partial x} + \frac{1}{3} \mu \frac{\partial^2 \hat{v}}{\partial x \partial y} - \hat{\rho}_0 \frac{\partial \hat{u}_0}{\partial y} \hat{v}$$

$$\hat{v}: \quad \nabla \cdot \left(- \begin{pmatrix} \mu + \varepsilon_2 & 0 \\ 0 & \frac{4}{3}\mu + \varepsilon_2 \end{pmatrix} \nabla \hat{v} \right) \; + \; \hat{\rho}_0 (\hat{u}_0 \; \hat{v}_0) \cdot \nabla \hat{v} + \hat{\rho}_0 \left(\frac{\partial \hat{v}_0}{\partial y} - i\omega \right) \hat{v} \; =$$

$$= - \frac{\partial c^2 \hat{\rho}}{\partial y} - \left(\hat{u}_0 \frac{\partial \hat{v}_0}{\partial x} + \hat{v}_0 \frac{\partial \hat{v}_0}{\partial y} \right) \hat{\rho} - \hat{\rho}_0 \frac{\partial \hat{v}_0}{\partial x} \hat{u} + \frac{1}{3} \mu \frac{\partial^2 \hat{u}}{\partial x \partial y}$$

Density perturbations

f = 800 Hz

Both acoustic and vorticity perturbations

$$\rho'(\boldsymbol{x},t) = \mathrm{Re}\{\rho(\boldsymbol{x},\omega)\exp(-i\omega t)\}$$

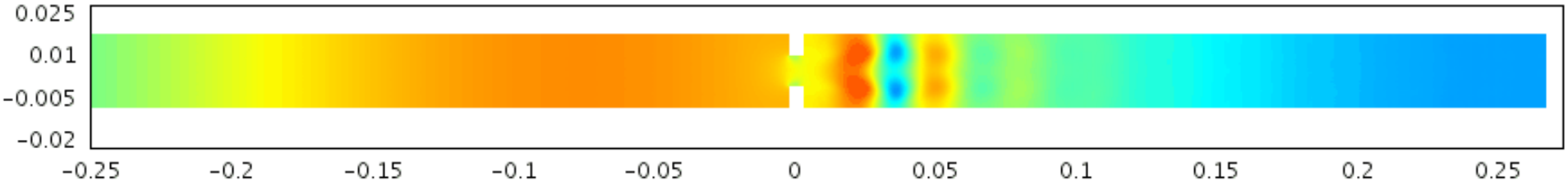

Single frequency calculations.
Frequency sweep $100 < f < 5000$ Hz, $\Delta f = 100$ Hz.

Finite Element Method (FEM). COMSOL Multiphysics.
10 000 elements, 3rd order shape functions.
280 000 Degrees of Freedom / calculation.

Scattering matrix

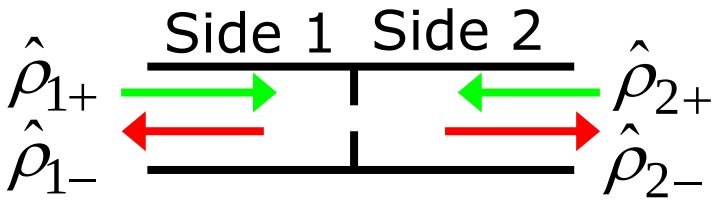

$$\begin{pmatrix} (1+M)\,\hat{\rho}_{2-} \\ (1-M)\,\hat{\rho}_{1-} \end{pmatrix} = \begin{pmatrix} T^{+} & R^{-} \\ R^{+} & T^{-} \end{pmatrix} \begin{pmatrix} (1+M)\,\hat{\rho}_{1+} \\ (1-M)\,\hat{\rho}_{2+} \end{pmatrix}$$

- Relates outgoing waves to incident waves.
- Every matrix element is a funtion of frequency.
- Works only in the plane-wave regime!

Scattering matrix, results (M=0.044)

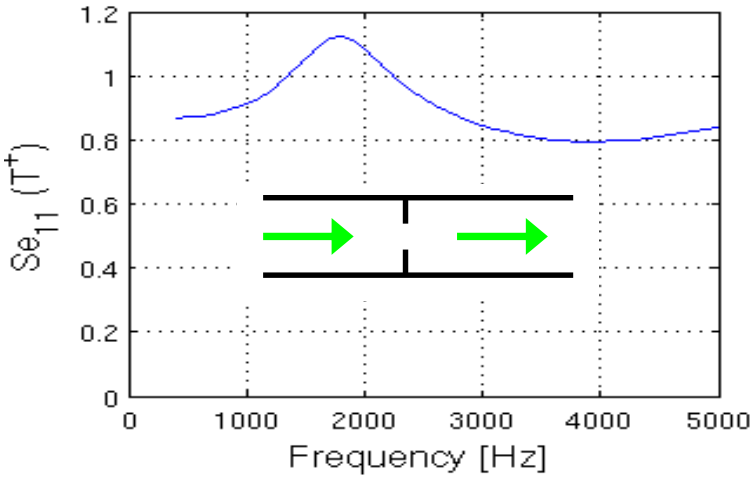

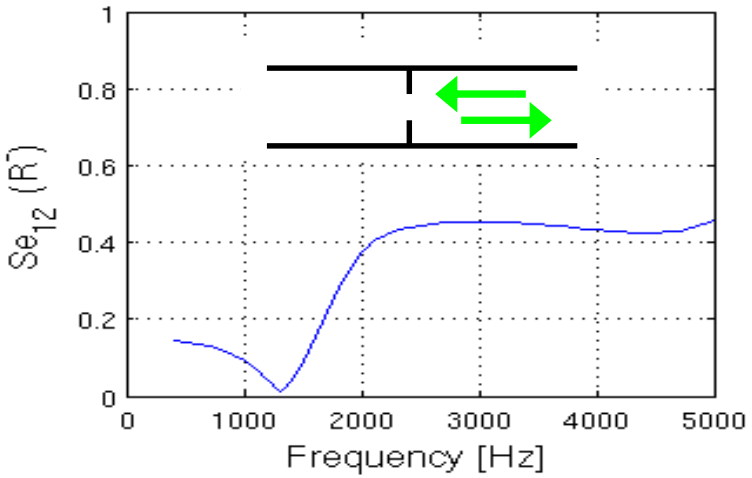

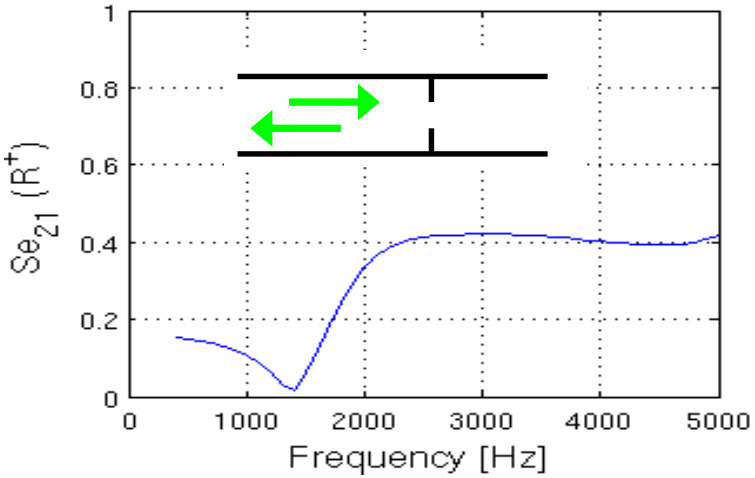

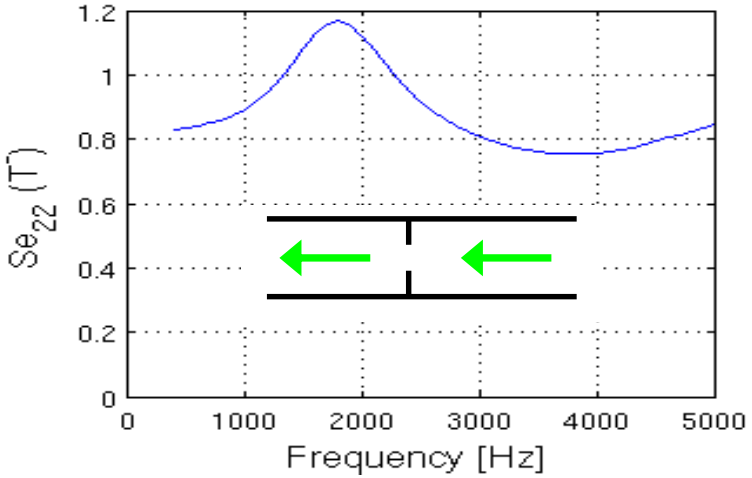

Whistling potentiality (POWER AMPLIFICATION)

Power balance

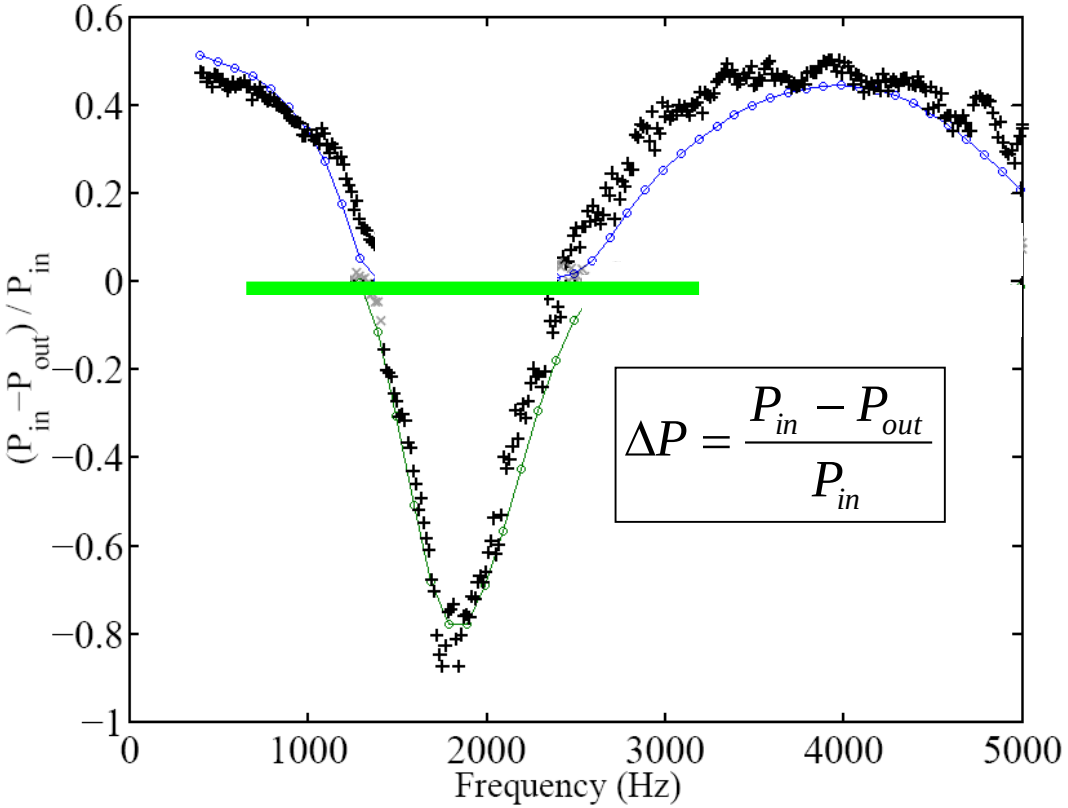

- Measurements: Testud et al. (JSV 2009)

Whistling setup

ROYAL INSTITUTE OF TECHNOLOGY

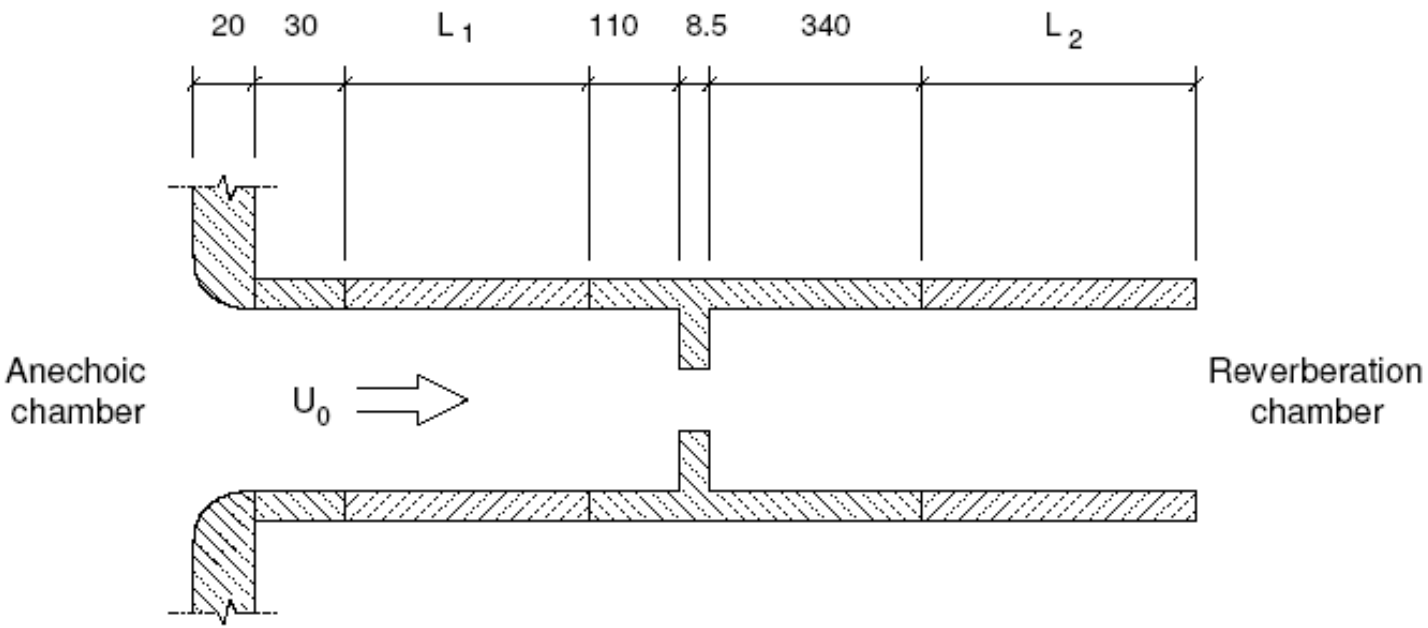

Nyquist (plot of det(E-SR)=0)*

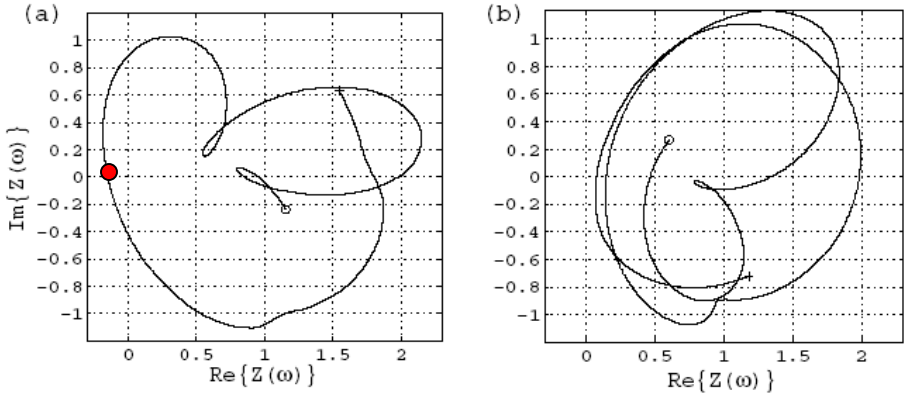

From Ref. [7].

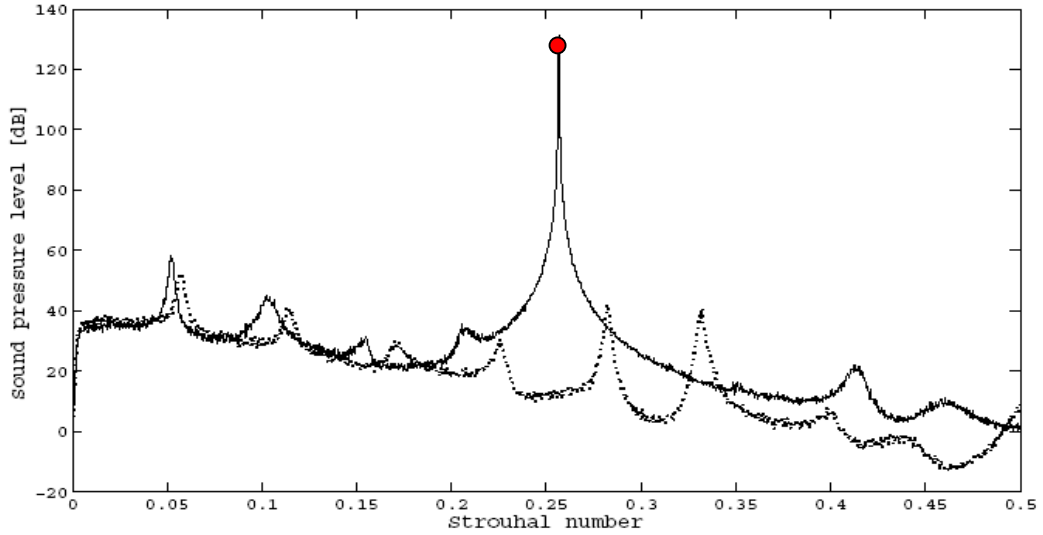

*) K. Karlsson and M. Åbom (2011), On the use of linear acoustic multi-ports to predict whistling in confined flows. Acta Acustica united with Acustica 97(1), 24-33.

ROYAL INSTITUTE OF TECHNOLOGY

Single Orifice ii) Complete 2-port (plane wave range) using LES [8,9]

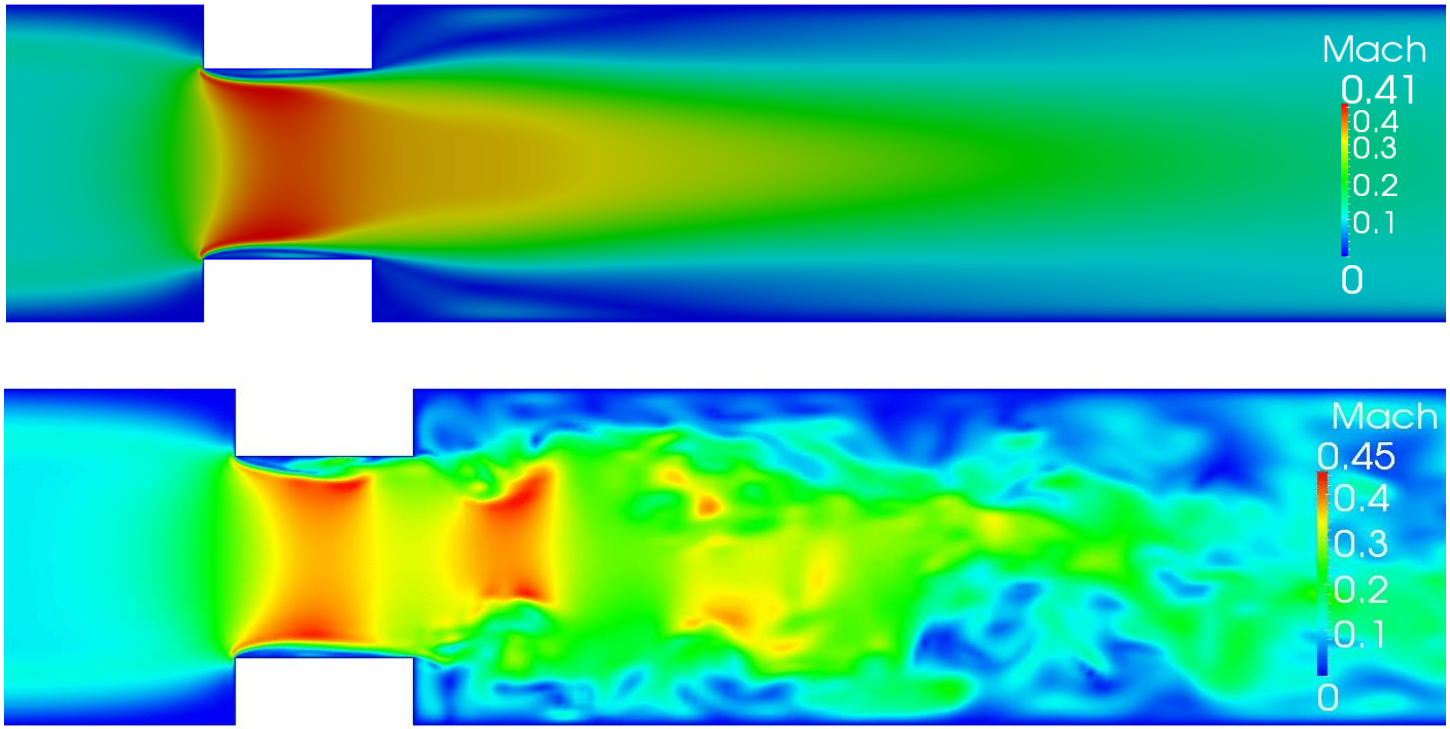

Orifice thickness 20 mm, Diameter 24 mm. Two duct cross-sections: circular and square. Area contraction ratio 0.36. Sound speed 343 m/s. Mach number 0.09, Re-number 80,000.

Scattering matrix, M=0.09 [8,9]

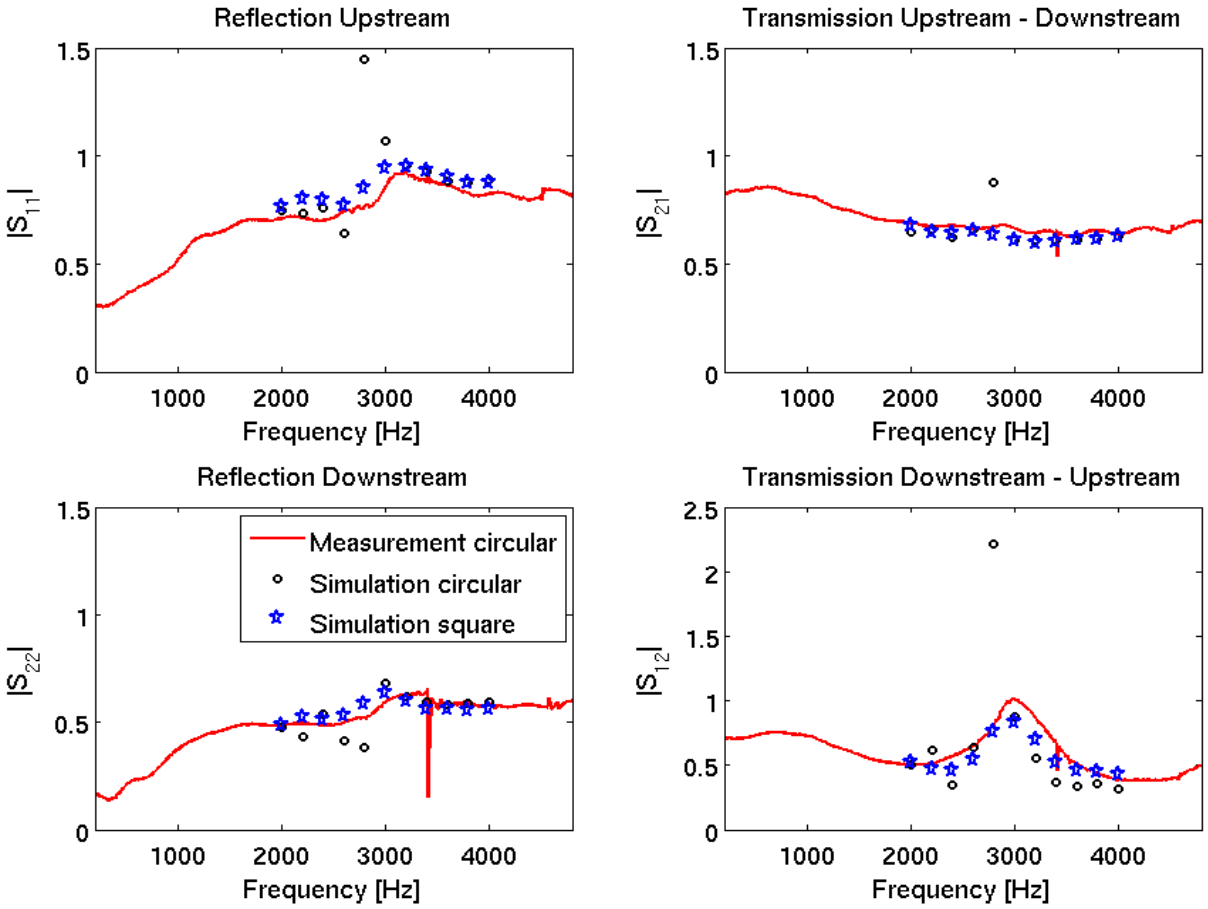

Scattering matrix, M=0.09 [8,9]

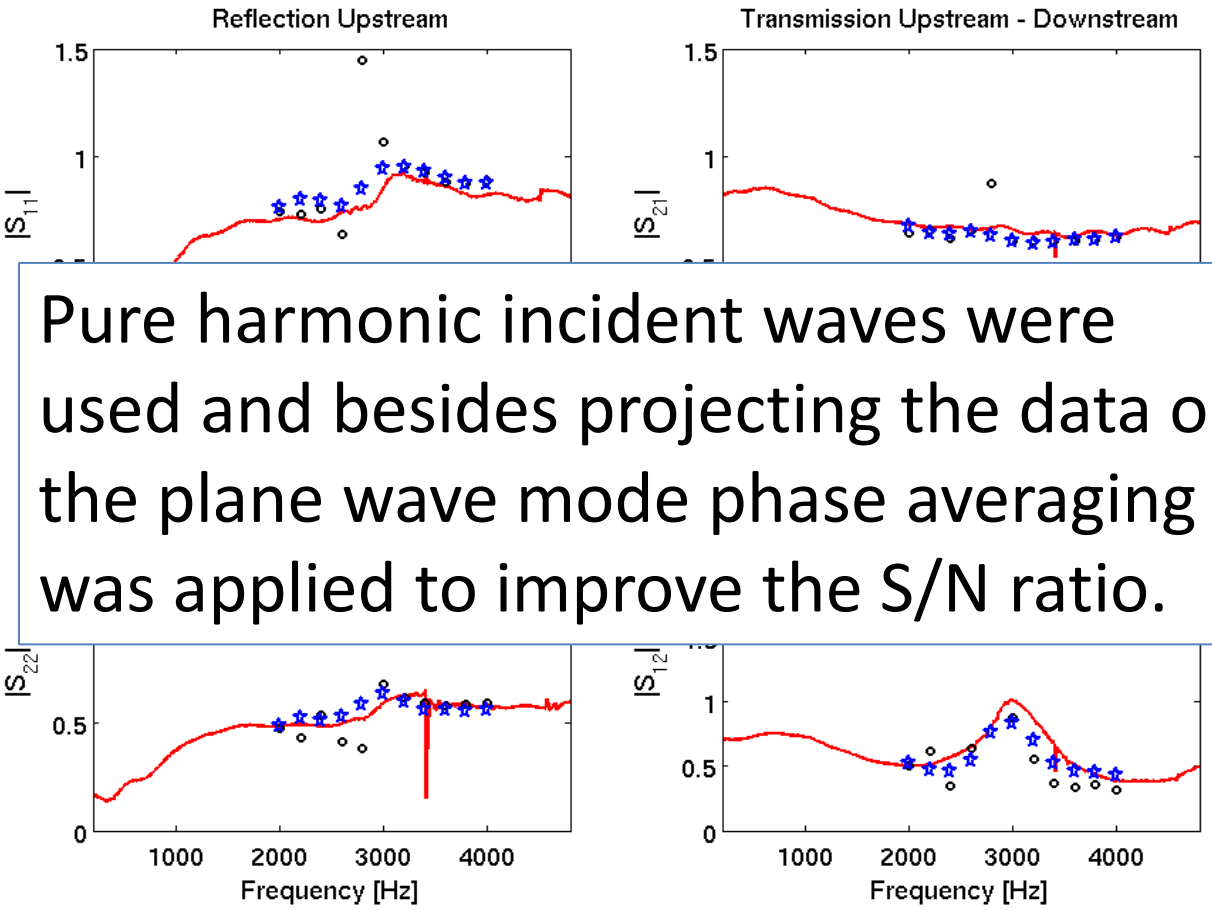

Pure harmonic incident waves were used and besides projecting the data on the plane wave mode phase averaging was applied to improve the S/N ratio.

Source strength, M=0.09 [8]

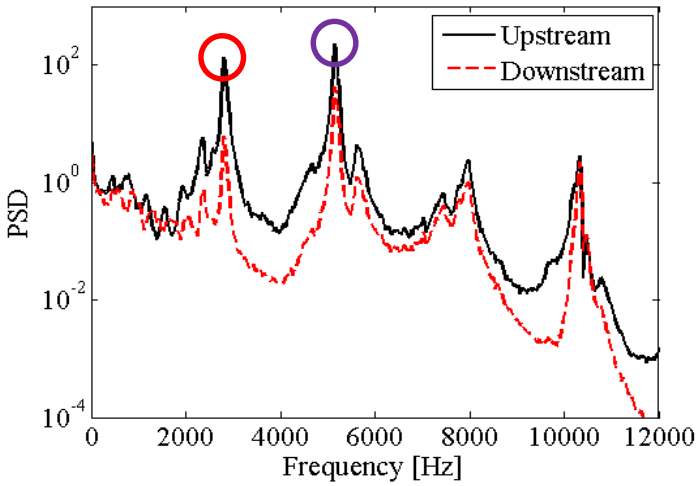

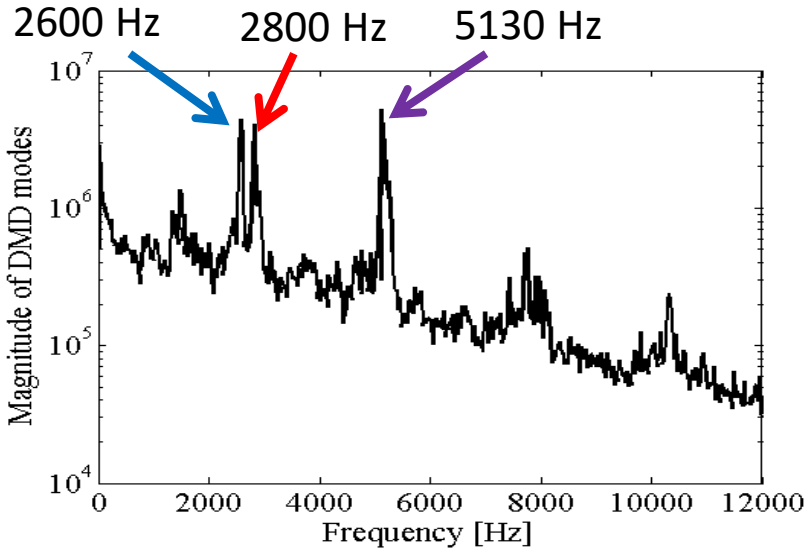

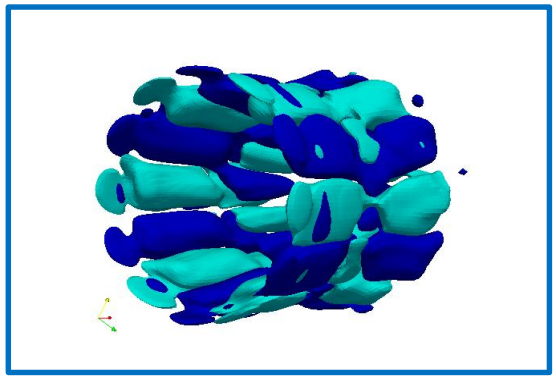

DMD = Dynamic or so called Koopman modes

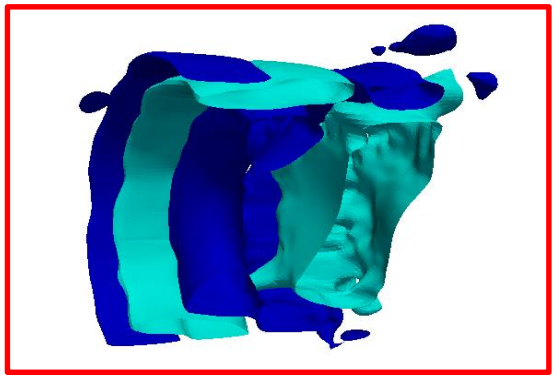

Source strength, M=0.09 [8]

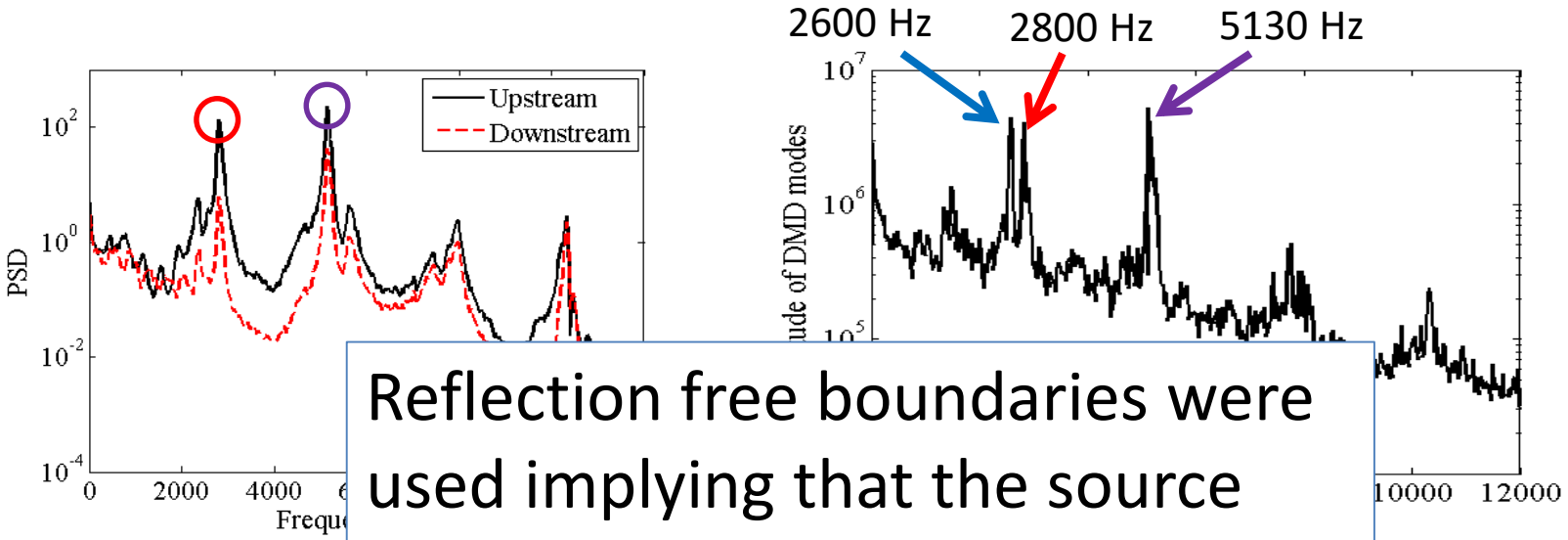

Reflection free boundaries were used implying that the source data could be directly computed.

$$\mathbf{p}_{s+} = \mathbf{p}_{+} - \mathbf{S}\mathbf{p}_{-}$$

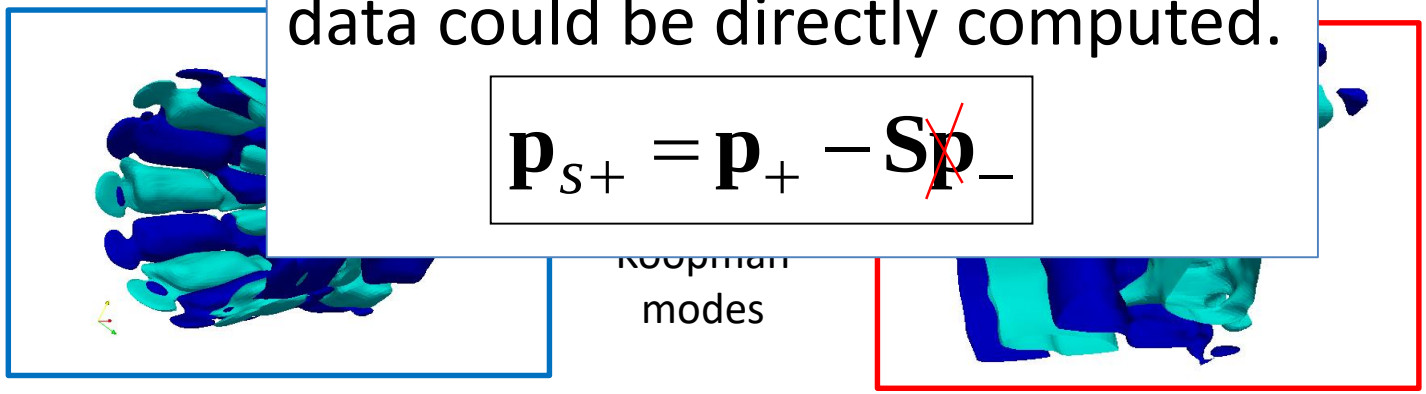

Aeroacoustic response of a T-junction [10]

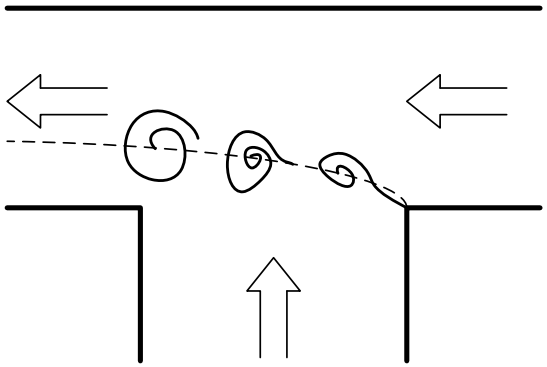

T-junction with open ends
in a pipe network and mixed grazing&bias flow conditions

Experimental set-up

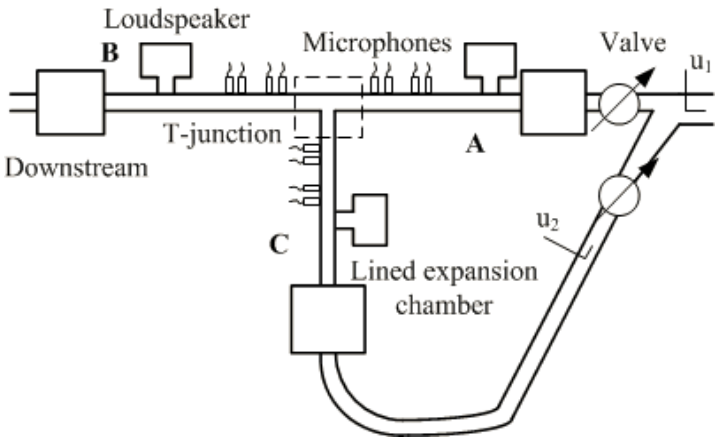

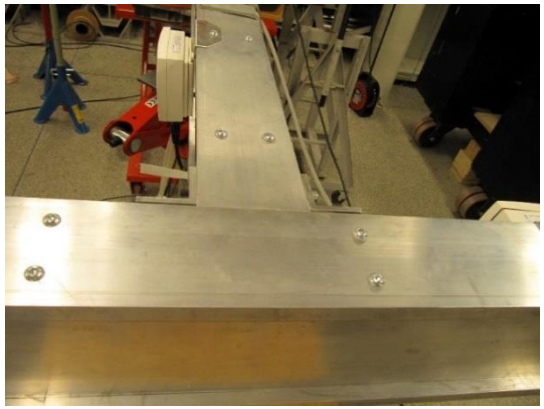

Possible phenomena:

- Sound attenuation
- Sound generation

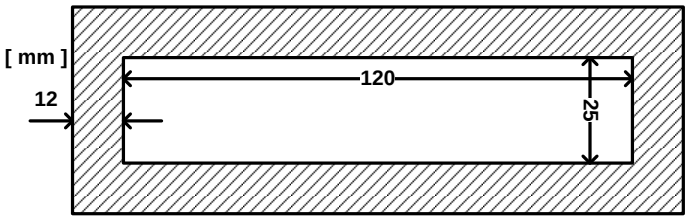

N.B. The three ducts forming the junction were equal

Plane waves = 3-port scattering matrix

$$\mathbf{p}_+ = \mathbf{S}\mathbf{p}_- + \mathbf{p}_+^s$$

$$\mathbf{S} = \begin{bmatrix} R_I & T_{II,I} & T_{III,I} \\ T_{I,II} & R_{II} & T_{III,II} \\ T_{I,III} & T_{II,III} & R_{III} \end{bmatrix}$$

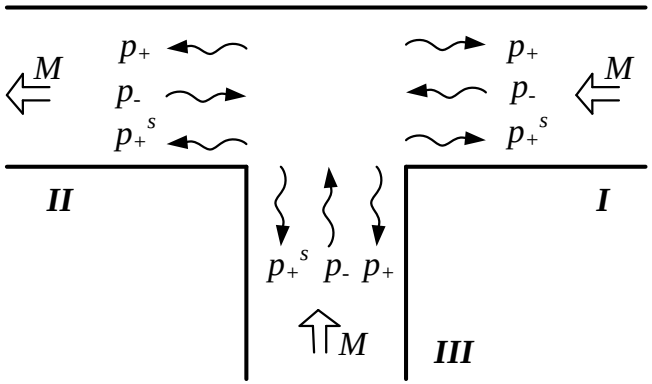

$\mathbf{p}_-$ Incoming acoustic waves;

$\mathbf{p}_+$ Outgoing acoustic waves;

$\mathbf{p}_+^s$ Acoustic waves independent on the incoming waves.

Example: Power balance sound incident from branch III

$$\mathbf{S} = \begin{bmatrix} R_I & T_{II,I} & T_{III,I} \\ T_{I,II} & R_{II} & T_{III,II} \\ T_{I,III} & T_{II,III} & R_{III} \end{bmatrix}$$

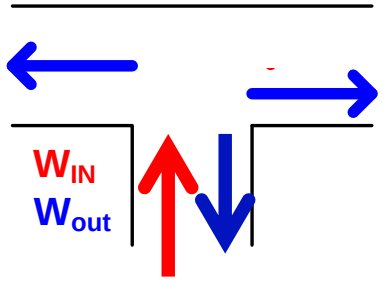

$$\frac{\langle W_{out}^{III} \rangle}{\langle W_{in}^{III} \rangle} = \frac{|R_{III}|^2 (1-M_{III})^2}{(1+M_{III})^2} + \frac{|T_{III,II}|^2 (1+M_{II})^2}{(1+M_{III})^2} + \frac{|T_{III,I}|^2 (1-M_I)^2}{(1+M_{III})^2}$$

$$\frac{\langle W_{out}^{III} \rangle}{\langle W_{in}^{III} \rangle} < 1 \Rightarrow \text{ Dissipation}$$

$$\frac{\langle W_{out}^{III} \rangle}{\langle W_{in}^{III} \rangle} > 1 \Rightarrow \text{ Amplification}$$

Numerical method 2D Linearized Navier Stokes Equations in frequency domain

Mean flow: RANS k-ε model

Acoustic field: LNSE

Continuity equation

$$-i\omega\hat{\rho} + \hat{\rho}\frac{\partial u_{0k}}{\partial x_k} + u_{0k}\frac{\partial \hat{\rho}}{\partial x_k} = -\frac{\partial \rho_0 \hat{u}_k}{\partial x_k}$$

Momentum equation

$$u_{k0}\frac{\partial \hat{u}_i}{\partial x_k} + \frac{\partial u_{0i}}{\partial x_k}\hat{u}_k - i\omega\hat{u}_i = -\frac{c^2}{\rho_0}\frac{\partial \hat{\rho}}{\partial x_i} + (\nu + \nu_\tau)\left[\frac{\partial^2 \hat{u}_i}{\partial x_j \partial x_j} + \frac{\partial^2 \hat{u}_j}{\partial x_i \partial x_j} - \frac{2}{3}\frac{\partial\left(\frac{\partial \hat{u}_k}{\partial x_k}\delta_{ij}\right)}{\partial x_j}\right]$$

N.B. Here the effect of eddy viscosity has been added to the model as described in A. Holmberg, A. Kierkegaard, C.Weng, A frequency domain linearized Navier-Stokes method including acoustic damping by eddy viscosity using RANS, J. Sound. Vib. 346 (2015), 229-247.

Mean flow based on RANs (Mg=0.1)

$M_b = 0.00$

$M_b = 0.015$

Turbulence viscosity

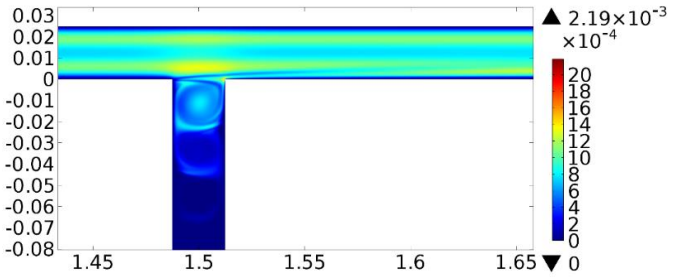

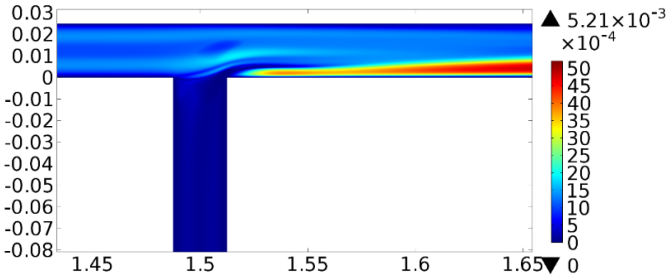

Velocity in x-direction

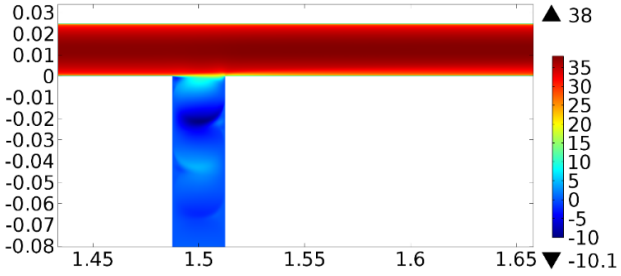

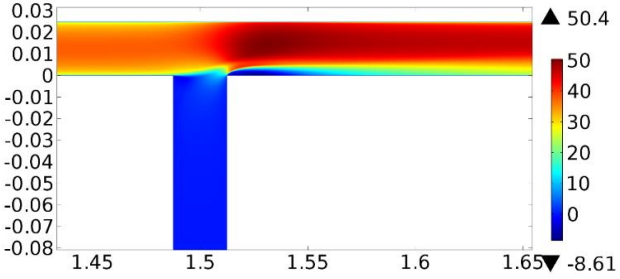

Power balance of different bias flow (Mg=0.1)

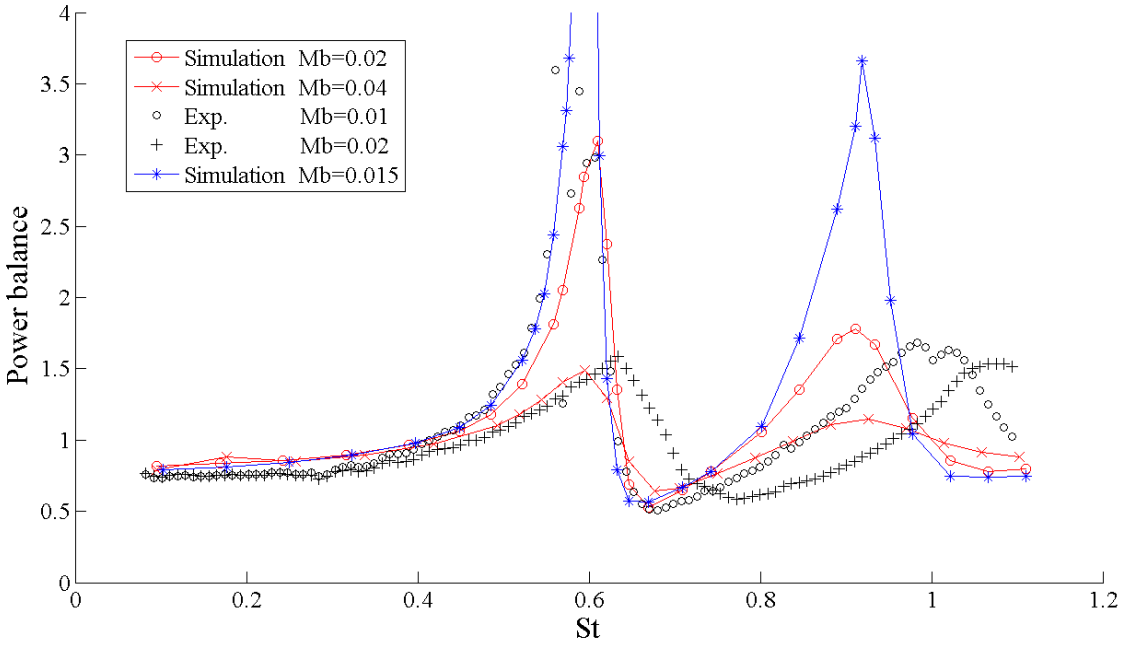

Sound excited in the side-branch

Integrated DEsign of OptimAL VENTilation Systems for Low Cabin and Ramp Noise [12-14]

www.idealvent.eu

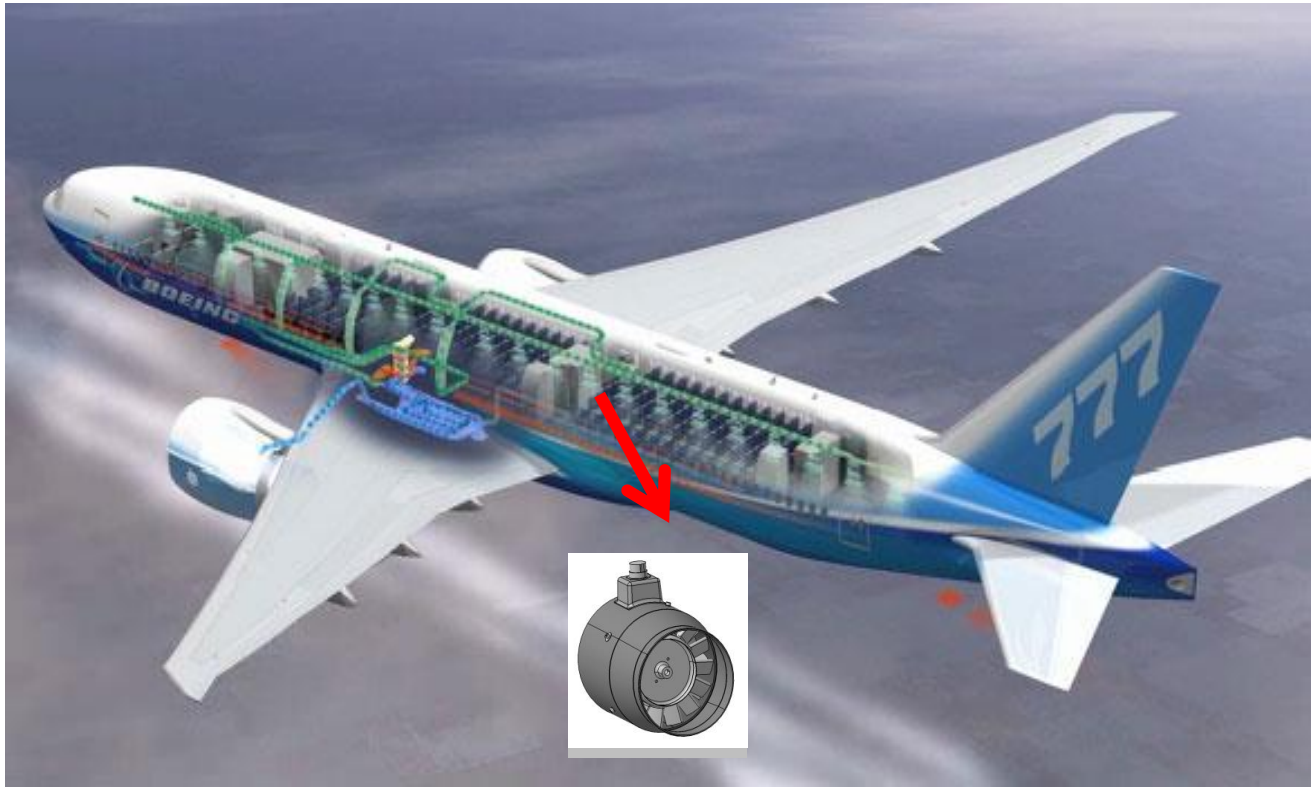

Objectives [12,13]

Investigating the **effect of installation (acoustic & aerodynamic)** on the **acoustic properties** of induct orifice plates (separation 2D, 4D and 9D)

The problem is simplified to a **single (clean) orifice** and a **tandem – orifice** configuration

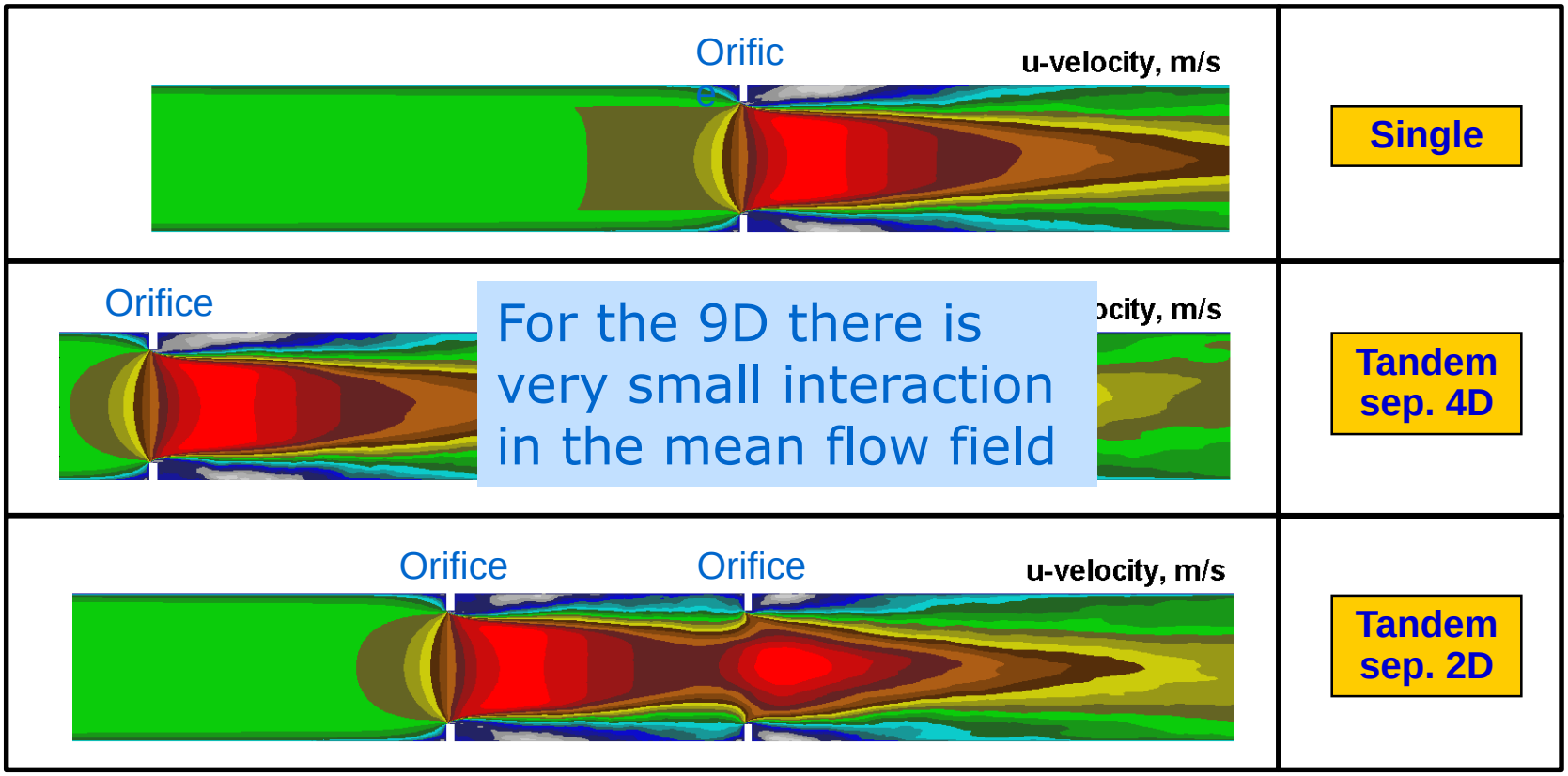

Objectives [12,13]

The problem is split into the following parts:

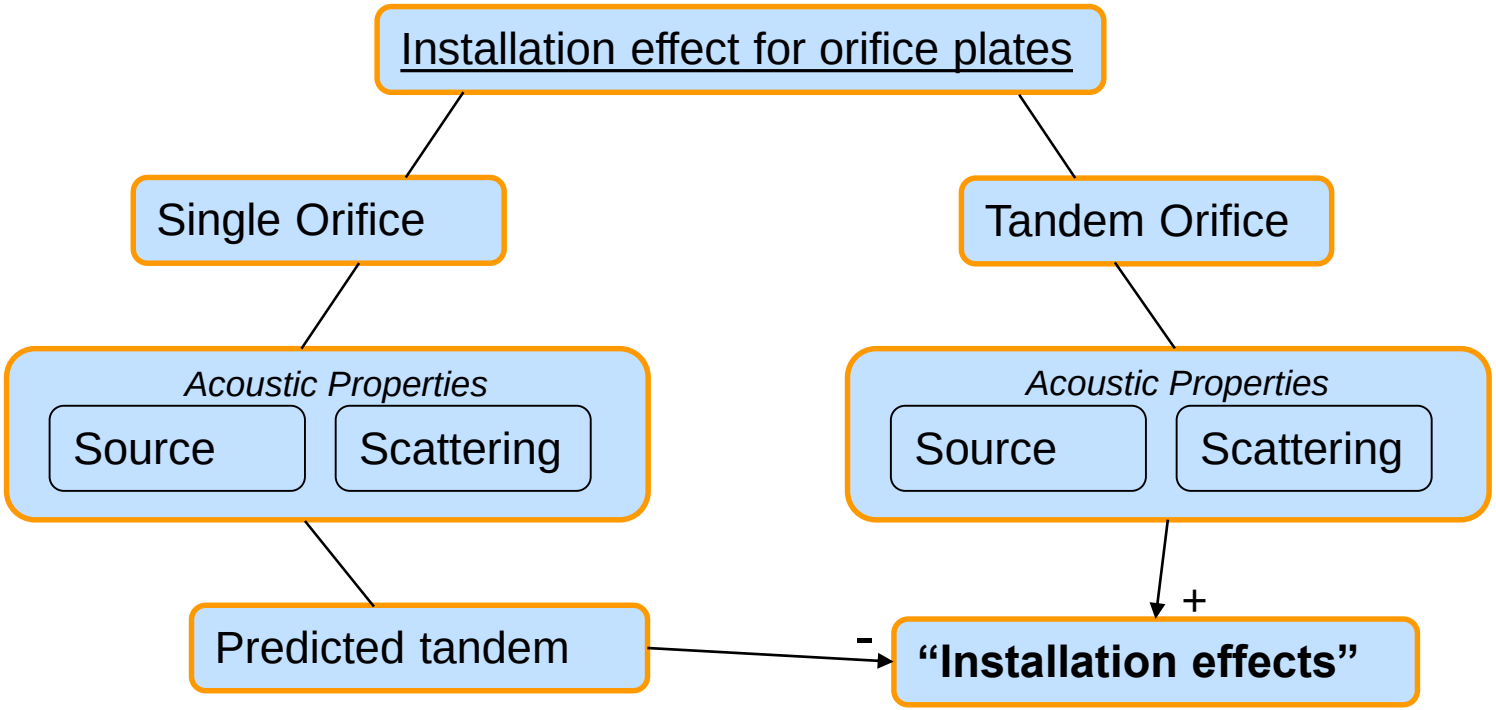

The **installation effects** will simply be **the difference** between ‘predicted’ and ‘real’.

The **Scattering Matrices** should “handle” the acoustic installation effects **BUT** the multi-port **Source strength** assumes an undisturbed inflow….

Objectives [12,13]

The problem is split into sub problems

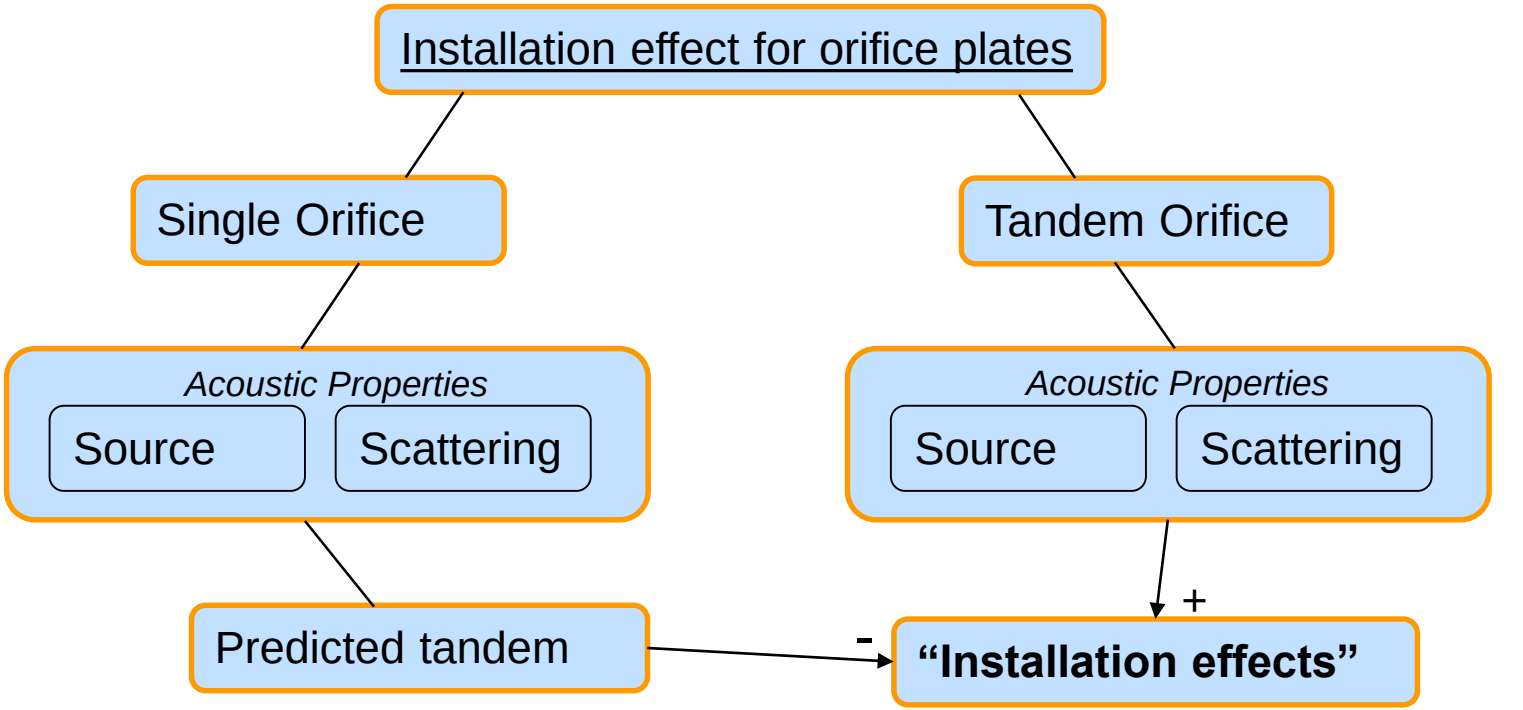

Orifice Measurements

Measurements for model-validation at the *Marcus Wallenberg Laboratory for Sound and Vibration Research at KTH*

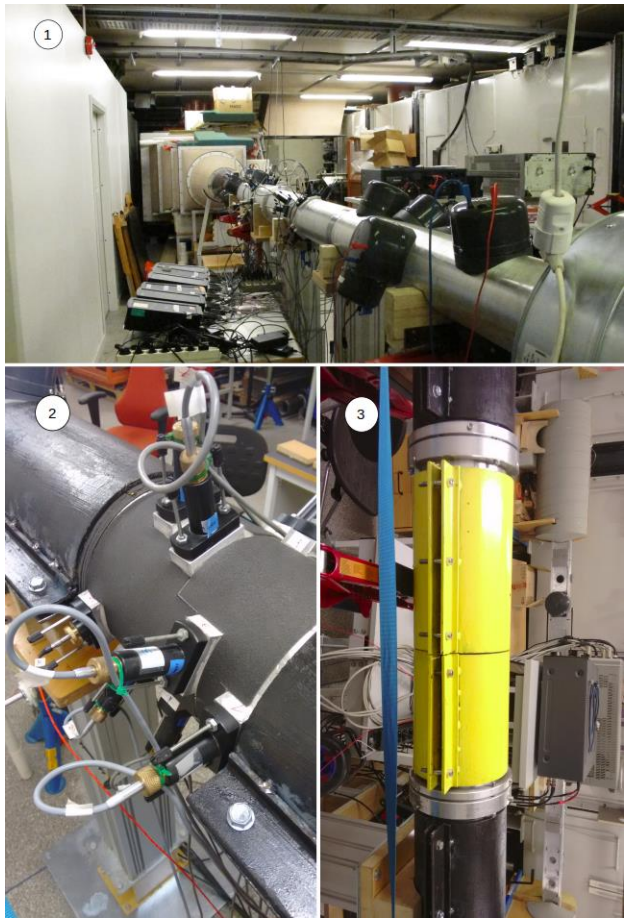

- **24 microphones** and **16 loudspeakers** in an optimised setup
- Aluminum pipe-sections with **constraint layer damping**
- Multi-channel excitation with algorithms for **simultaneous, uncorrelated excitation**
- **Modal decomposition** with wave-numbers including visco-thermal damping
- Two stage measurements for **accurate scattering** and **source** characterisation

Sack, S., **Åbom**, M., & **Efraimsson**, G. (2016).

On Acoustic Multi-Port Characterisation Including Higher Order Modes.

Acta Acustica United with Acustica, *102*, 834–850.

Orifice Computations (Unsteady Flow)

Hybrid RANS-LES method (IDDES), NTS

- General approach: Direct computations of pressure fields generated by the orifice on the basis of **compressible scale-resolving simulations of the turbulence** with the use of **hybrid RANS-LES method** (IDDES)
  - Combined with Volumetric **Synthetic Turbulence Generator (VSTG)** for "injection" of turbulent content upstream of the noise-generating area
  - Inflow / outflow BCs for IDDES are set based on 2 auxiliary stages
    - 1. Precursor steady RANS of the inlet part of the duct: inflow profiles
    - 2. Precursor RANS of diaphragm(s) flow: used to impose outflow BCs

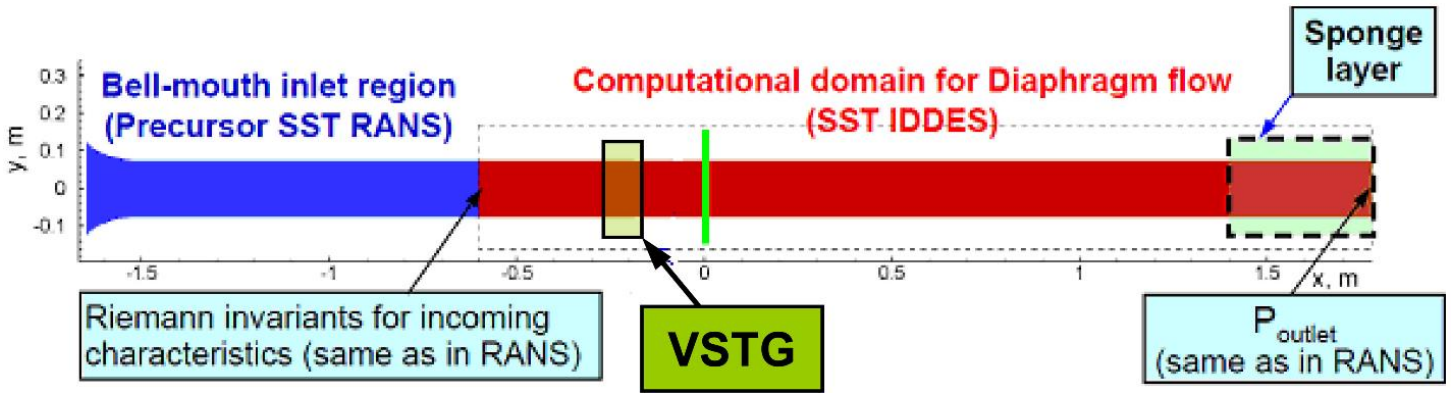

Orifice Computations (Scattering)

Linearised Navier Stokes Eq. (LNSE), KTH

Linearised Navier Stokes Equations in the frequency domain

$$i\omega\rho + \nabla\cdot(\rho\mathbf{u}_0 + \rho_0\mathbf{u}) = M$$

(1) Mass

$$\rho_0\left(i\omega\mathbf{u} + (\mathbf{u}\cdot\nabla)\mathbf{u}_0 + (\mathbf{u}_0\cdot\nabla)\mathbf{u}\right) - \nabla\cdot\boldsymbol{\sigma} = \mathbf{F}$$

(2) Momentum

$$\rho_0 C_p\left(i\omega T + (\mathbf{u}\cdot\nabla)T_0 + (\mathbf{u}_0\cdot\nabla)T\right) + \rho C_p(\mathbf{u}_0\cdot\nabla)T_0$$
$$-\alpha_0 T_0\left(i\omega p + (\mathbf{u}\cdot\nabla)p_0 + (\mathbf{u}_0\cdot\nabla)p\right) - \alpha_0 T(\mathbf{u}_0\cdot\nabla)p_0 - \nabla\cdot(k\nabla T) = \Phi + Q$$

(3) Energy

$$\boldsymbol{\sigma} = -p\mathbf{I} + \mu(\nabla\mathbf{u} + (\nabla\mathbf{u})^{\mathrm{T}}) + \left(\mu_B - \frac{2}{3}\mu\right)(\nabla\cdot\mathbf{u})\mathbf{I}$$

$$\rho = \rho_0(\beta_T p - \alpha_0 T)$$

Background mean flow is computed using RANS, different turbulence models are tested (ongoing work)

similar procedure as for **measurements**, but with higher number of sampling points

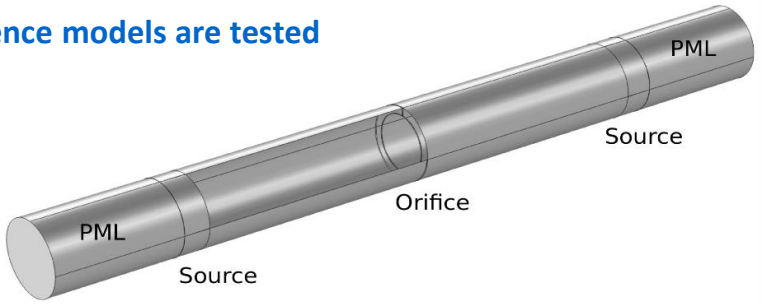

For Linearized-Navier-Stokes solver for acoustic plane wave modes see:
Kierkegaard et al. *(2012). Simulations of whistling and the whistling potentiality of an in-duct orifice with linear aeroacoustics.* Journal of Sound and Vibration.

Single Orifice Scattering

Linearised Navier Stokes Eq. (LNSE), KTH

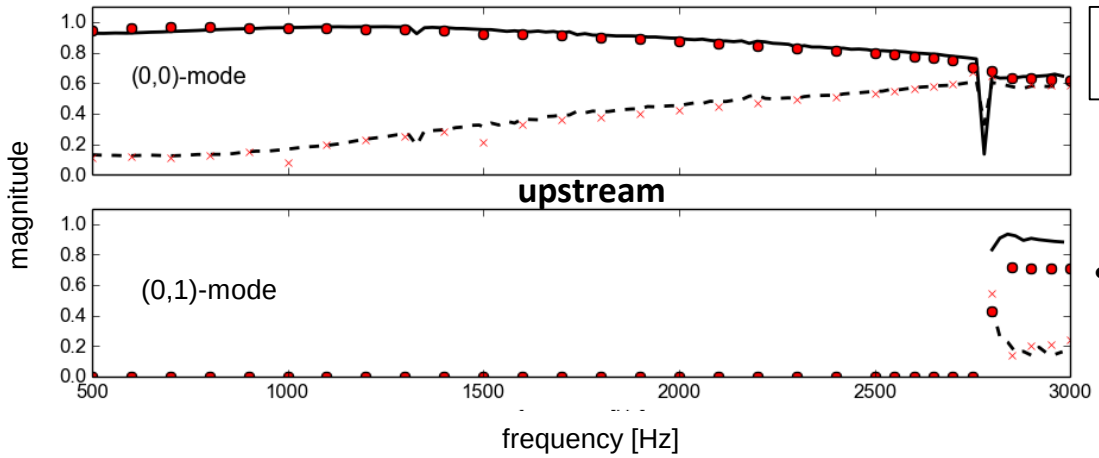

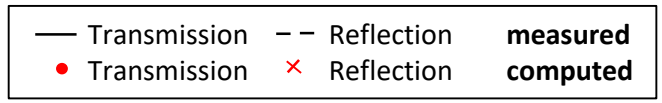

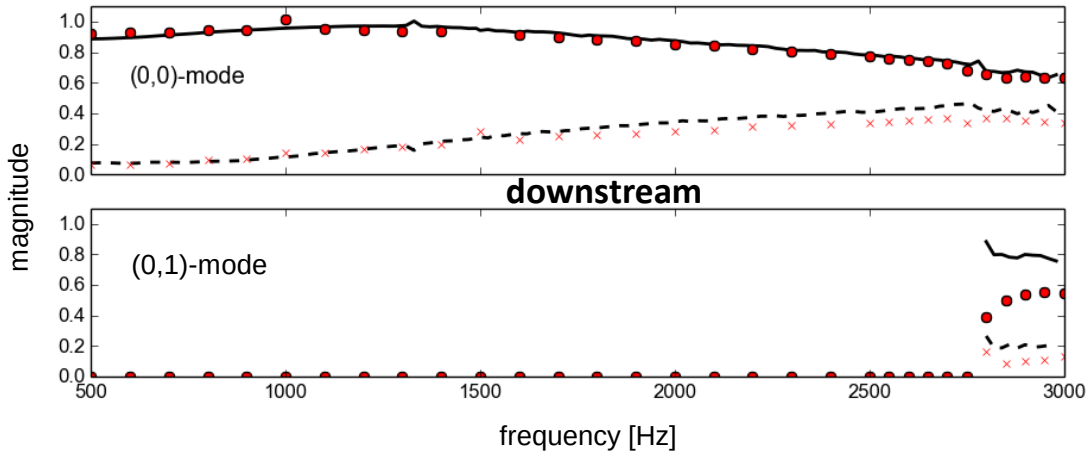

- Transmission and Reflection of the plane wave is captured well (upstream).
- Reflection of the plane wave downstream and transmission of the (0,1) modes are too low, upstream and downstream.

$$\Psi_{n+} \neq \Psi_{n-}$$

60

Post-processing: Tandem Scattering

Multi-Port Networks, KTH

Combining two multi-ports is a **multiplication** of their **transfer matrices**
Computing the **transfer matrix** is a **linear operation** on the scattering matrix

➡ **computational inexpensive**

2D distance

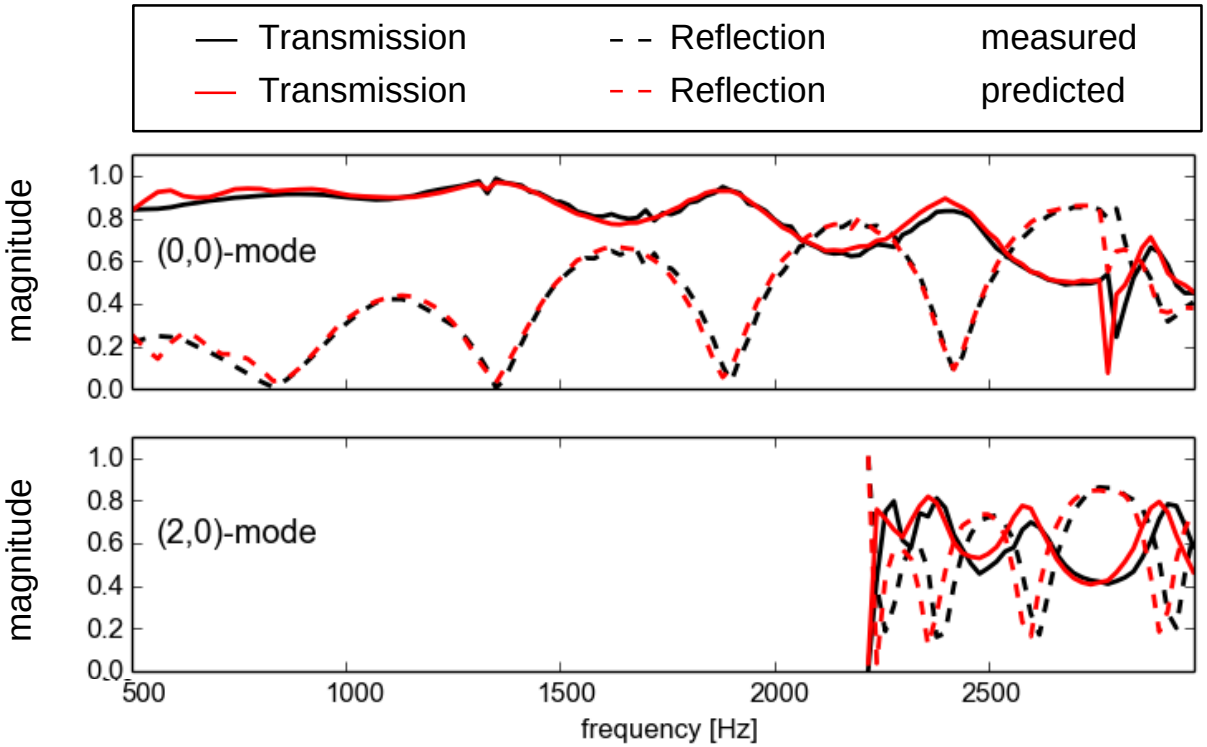

The sound scattering of an orifice plate is very little effected by disturbed inflow

61

Post-processing: Source strength

Mode decomposition for modal source power, KTH, NTS

The **'raw' pressure fluctuations** contain **the acoustic signal**, but **covered** by **'hydrodynamic noise'** that is not part of the acoustics

Approach:

The **hydrodynamic fluctuations are only locally correlated**
Projection on the acoustic modes and cross-correlating points at "large" separations removes this uncorrelated part of the signal. Note in this case the CFD model was **not reflection-free** so one must use the Scattering matrix to remove reflections.

Cross correlation of 4 decomposition zones with 250 points each (correlation matrix [500x500])

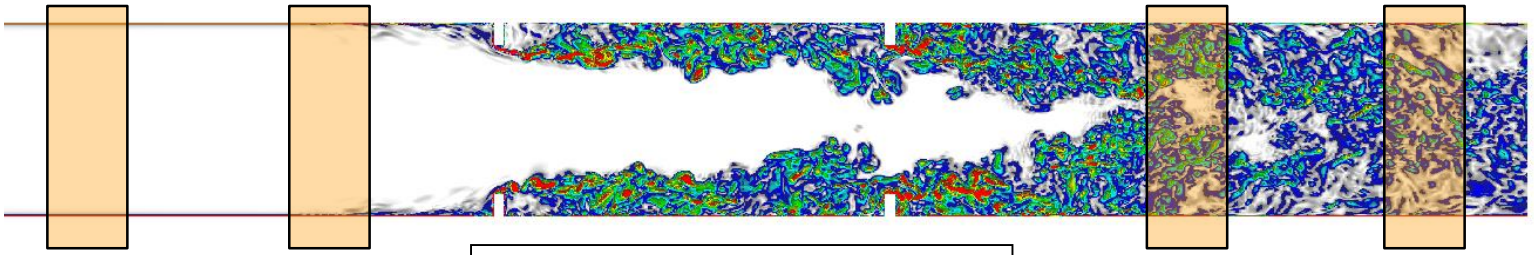

$$\mathbf{p}_{s+} = \mathbf{p}_{+} - \mathbf{S}\mathbf{p}_{-}$$

62

Single Orifice Source strength

Mode decomposition for modal source power, KTH, NTS

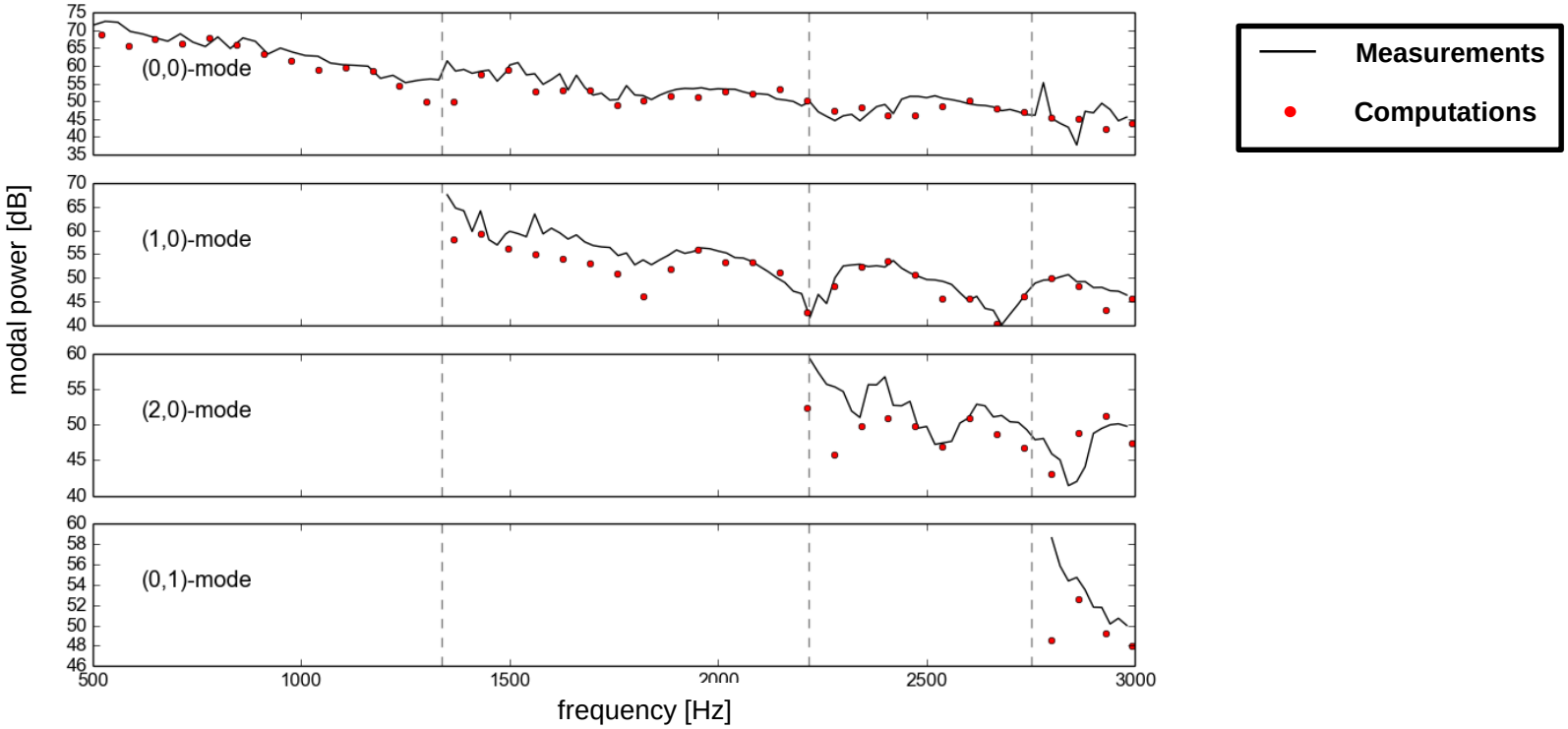

- The agreement is good for all modes and the total levels could be predicted within a few dB.

Post-processing: Tandem Source

Multi-Port Networks, KTH

For the source, the power **cross spectrum is computed**, **neglecting correlated sound sources** between the two multi-ports

➡ This will cause aerodynamic installation effects when the flow fields interact”

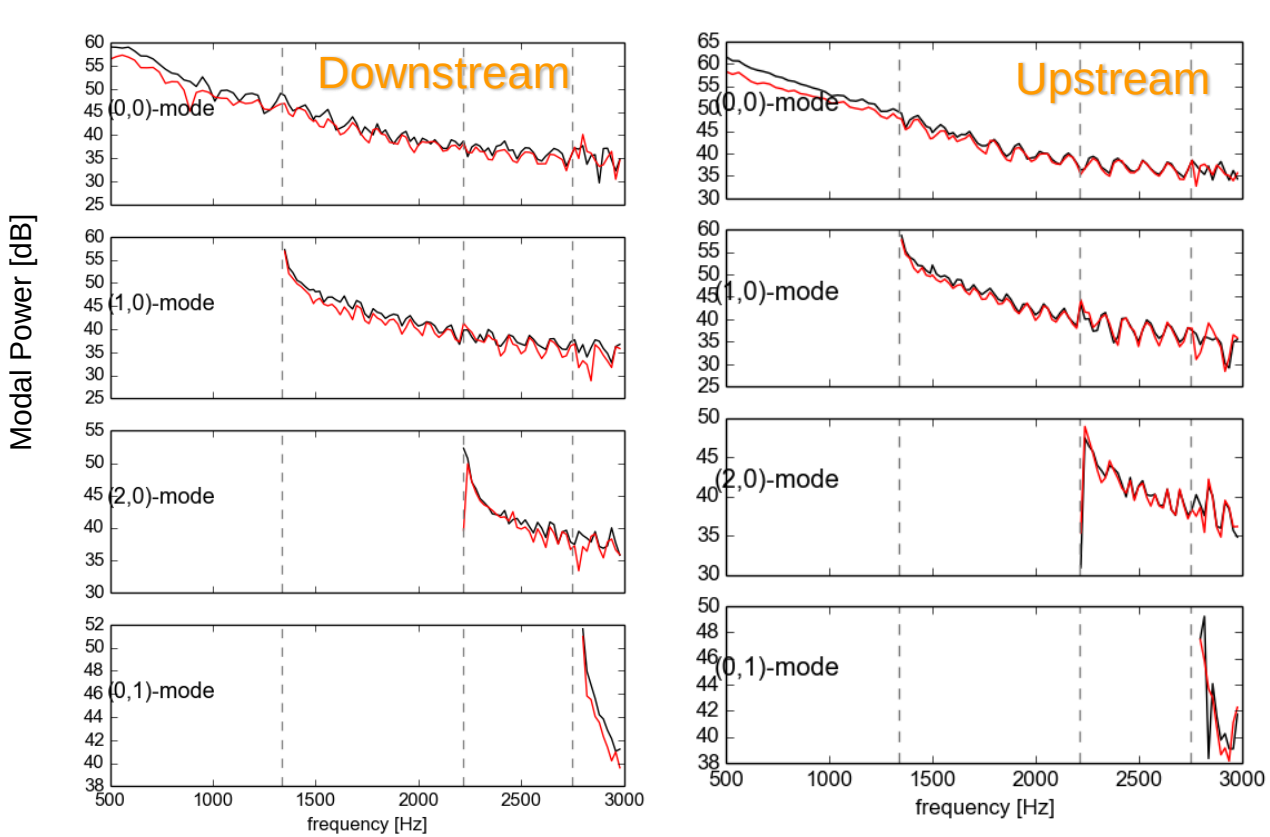

Only very good agreement for the long separation (9D)

SUMMARY

- Multi-port models have traditionally been associated with experiments but a growing trend the last 10 years is to determine multi-port data by CFD models.

- The basis for multi-port models is to project the field on acoustic modes which will reduce hydrodynamic noise (turbulence/vorticity) in the data.

- The multi-port procedure will create reflection free data which makes it ideal for comparing numerical/experimental work.

- Multi-port models are also excellent to analyse cases where flow-sound interactions, e.g., vortex-sound effects, are important (orifice plates, T-junctions,…).

- This opens the possibility to predict amplification of sound and by a system stability analysis find unstable eigen-frequencies (“whistling”).

Reference list

1. Bodén, H. and Åbom, M., 1995. Modelling of fluid machines as sources of sound in duct and pipe systems. Acta Acustica 3, Dec., pp. 1-12.
2. J. Lavrentjev, M. Åbom and H. Bodén, 1995, A measurement method for determining the source data of acoustic two-port sources. *Journal of Sound and Vibration* 183, 517-531.
3. J. Lavrentjev and M. Åbom, 1995. A measurement method to determine the source-data of acoustic N-port sources. *Journal of Sound and Vibration* 197, 1-16.
4. M Karlsson, M Åbom (2010). Aeroacoustics of T-junctions –An experimental investigation. *Journal of Sound and Vibration* 329 (10), 1793-1808.
5. A. Holmberg, M. Åbom and H. Bodén (2011), "Accurate experimental two-port analysis of flow generated sound". *Journal of Sound and Vibration*, DOI: 10.1016/j.jsv.2011.07.041.
6. A. Kierkegaard, S. Boij and G. Efraimsson (2010), "A frequency domain linearized Navier-Stokes equations approach to acoustic propagation in flow ducts with sharp edges", *J. Acoustical Soc. of America* 127, 710-719.
7. Kierkegaard, A., Allam, S., Efraimsson, G and Åbom, M. (2012). Simulations of whistling and the whistling potentiality of an in-duct orifice with linear aeroacoustics. Journal of Sound and Vibration 331, 1084–1096.

Reference list

8. Alenius, E. (2012) *Flow Duct Acoustics: An LES Approach*. PhD thesis, KTH The Marcus Wallenberg Laboratory for Sound and Vibration Research, Stockholm, Sweden.
9. Alenius E., Åbom M. and Fuchs L., 2015. Large eddy simulations of acoustic-flow interaction at an orifice plate. *Journal of Sound and Vibration*, Vol. 345, pp 162-177.
10. Du L., Holmberg A., Karlsson M. and Åbom M., 2016. Sound amplification at a rectangular T-junction with merging mean flows. Journal of Sound and Vibration, Vol. 367, pp 69-83.
11. Sack, S., Åbom, M. and Efraimsson, G., 2016. On acoustic multi-port characterization including higher order modes. Acta Acoustica united with Acustica, ISSN 1610-1928, Vol. 192, nr 5, 834-850.
12. Shur, M., Strelets, M., Travin, A., Christophe, J., Kucukcoskun, K., Schram, C., Sack, S., Åbom, M., 2017. Experimental/Numerical Study of Ducted-Fan Noise: Effect of Duct Inlet Shape. AIAA Journal 56 (3), 979-996.
13. Sack, S., Åbom, M., 2017. Investigation of orifice aeroacoustics by means of multi-port methods. Journal of sound and vibration 407, 32-45.
14. Sack, S., Shur, M., Åbom, M, Strelets. M., Travin, A., 2017. Numerical eduction of active multi-port data for in-duct obstructions. Journal of Sound and Vibration 411, 328-345.